


# Neutrino follow-up with the Zwicky Transient Facility: Results from the first 24 campaigns

Robert Stein <sup>1,2,3\*</sup>, and Growth Friends

<sup>1</sup>*Deutsches Elektronen-Synchrotron (DESY), Platanenallee 6, 15378 Zeuthen*

<sup>2</sup>*Institut für Physik, Humboldt-Universität zu Berlin, D-12489 Berlin, Germany*

<sup>3</sup>*Division of Physics, Mathematics, and Astronomy, California Institute of Technology, Pasadena, CA 91125, USA*

Accepted XXX. Received YYY; in original form ZZZ

## ABSTRACT

The Zwicky Transient Facility (ZTF) performs a systematic neutrino follow-up program, searching for optical counterparts to high-energy neutrinos with dedicated Target-of-Opportunity (ToO) observations. Since first light in March 2018, ZTF has taken prompt observations for a 24 high-quality neutrino alerts from the IceCube Neutrino Observatory, with a median latency of 12.2 hours from initial neutrino detection. From two of these campaigns, we have already reported tidal disruption events (TDEs) AT2019dsg and AT2019fdr as probable counterparts, suggesting that TDEs contribute  $>7.8\%$  of the astrophysical neutrino flux. We here present the full results of our program through to December 2021. No additional candidate neutrino sources were identified by our program, allowing us to place the first constraints on the underlying optical luminosity function of astrophysical neutrino sources. Transients with absolute magnitudes brighter than  $-21$  can contribute no more than  $87\%$  of the total, while transients brighter than  $-22$  can contribute no more than  $58\%$  of the total. These are the first observational constraints on the neutrino emission of populations such as superluminous supernovae. None of the neutrinos were coincident with bright optical AGN flares comparable to that observed for TXS 0506+056/IC170922A, suggesting that most astrophysical neutrinos are not produced during such optical flares. We highlight the outlook for electromagnetic neutrino follow-up programs, including the expected potential for the Rubin Observatory.

**Key words:** neutrinos – astroparticle physics – transients: tidal disruption events – transients: supernovae – gamma-ray bursts

## 1 INTRODUCTION

Astrophysical neutrinos are produced through the interaction of accelerated hadrons with matter or photons. A flux of high-energy astrophysical neutrinos was first discovered by IceCube in 2013 (IceCube Collaboration 2013). Recent results suggest that a substantial fraction of these neutrinos are produced in the cores of Active Galactic Nuclei (AGN) (Abbasi et al. 2021), with additional evidence for neutrino emission from the nearby AGN NGC 1068 (Aartsen et al. 2020). Beyond this static component, various transient or variable source classes have been proposed as possible contributors to the neutrino flux, including Gamma-Ray Bursts (GRBs) (Waxman & Bahcall 1997), Core-Collapse Supernovae (CCSNe) (Murase et al. 2011), TDEs (Farrar & Gruzinov 2009) and blazars (Mannheim 1993). All of these proposed neutrino source classes have electromagnetic signatures at optical wavelengths.

To aid in identifying these time-varying source candidates, IceCube has operated an automated program since 2016 to publish realtime high-energy neutrino alerts (Aartsen et al. 2017), enabling contemporaneous electromagnetic observations of putative neutrino source candidates at radio (Kadler et al. 2021a), optical (Kowalski &

Mohr 2007; Aartsen et al. 2015; Pan-Starrs Collaboration et al. 2019; Morgan et al. 2019; Lipunov et al. 2020; Necker et al. 2022), X-ray (Evans et al. 2015; Ferrigno et al. 2021), and gamma-ray wavelengths (Lucarelli et al. 2019; Garrappa et al. 2021b; Satalecka et al. 2021). In 2017, this realtime program led to the identification of a flaring blazar, TXS 0506+056, as the likely source of high-energy neutrino IC170922A (IceCube Collaboration et al. 2018). Studies of these high-energy neutrino alerts have suggested possible correlations with blazar sub-populations, namely radio-bright blazars (Plavin et al. 2020, 2021) and intermediate-energy/high-energy peaked blazars (IBLs/HBLs) (Giommi et al. 2020a).

The Zwicky Transient Facility (ZTF) is an optical telescope with a 47 sq. deg field of view (Bellm et al. 2019). Since first light in 2018, ZTF has operated a dedicated neutrino follow-up program, in which the arrival directions of IceCube neutrino alerts are observed with Target-of-Opportunity (ToO) observations (Graham et al. 2019). This program has led to the identification of two further likely high-energy neutrino sources, the TDE AT2019dsg (Stein et al. 2021a) and the probable TDE AT2019fdr (Reusch et al. 2021a). Accounting for the contribution of higher-redshift sources, these results suggest that at least  $7.8\%$  of neutrino alerts arise from the broader TDE population (Reusch et al. 2021a). Archival analysis of ZTF data

\* E-mail: rdstein@caltech.edu

revealed further evidence of a correlation between such flares and high-energy neutrinos (van Velzen et al. 2021).

In this paper we outline the full results of the ZTF neutrino follow-up program, which has to date included 24 dedicated neutrino follow-up campaigns. This sample enables novel constraints to be set on the neutrino emission of a broad range of optical transient and variable populations.

The paper is organised as follows: Section 2 outlines the program itself, including trigger criteria and optical candidate selection. Section 3 outlines transient candidates identified by the program, and subsequent electromagnetic observations to determine their nature. Section 4 outlines optical AGN flares found coincident with neutrinos, and Section 5 provides data on selected candidate neutrino sources identified in the literature. Section 6 considers the various constraints that can be placed on different possible neutrino source populations from our program. Section 7 summarises the main results, and outlines how such follow-up programs may improve with future observatories.

## 2 NEUTRINO FOLLOW-UP WITH ZTF

Neutrino alerts are generally published by IceCube in the form of automated Gamma-ray Coordination Network (GCN) Notices<sup>1</sup>, with initial estimates of the statistical uncertainty on the neutrino position. These positions are then superseded after a few hours by a GCN Circular with an updated localisation that also incorporates systematic uncertainties (Lagunas Gualda et al. 2021). Given the substantial increase in localisation area once systematic effects are accounted for, with increases of factor 5 not being uncommon, we rely on the latter category to perform our search for neutrino counterparts.

With ZTF, we aim to observe all accessible high-quality neutrino alerts from IceCube. We define high-quality alerts as those with a high probability to be of astrophysical origin (signalness > 50%), or those which are well-localised (a 90% localisation area < 10 sq. deg.). Though IceCube labels alerts as Gold or Bronze based on average quality, individual Bronze alerts have been reported with signalness values greater than 50% (e.g. IC211208A) and Gold alerts have been reported with signalness values less than 15% (e.g. IC201130A). We therefore ignore the labelling of these streams, and select exclusively based on the signalness and localisation.

We have followed up 24 neutrinos in the period from survey start on 2018 March 20 to 2021 December 31, out of a total of 79 neutrino alerts published by IceCube during that time. Table 1 summarises each neutrino alert observed by ZTF. From 2019 June 17, IceCube published neutrino alerts with improved selection criteria (V2) to provide an elevated alert rate (Blaufuss et al. 2019). In addition to 1 of the 12 alerts under the old selection, ZTF followed up 23 of the 67 alerts published under the V2 selection. Midway through the ZTF program, an additional cut on neutrino alert galactic latitude ( $|b| > 10$  deg) was introduced to avoid crowded fields with many stars.

Each neutrino localisation region can typically be covered by one or two observations of fields in a predefined ZTF ‘grid’ tiling of the sky. Multiple observations are scheduled for each field, with both  $g$  and  $r$  filters, and a separation of at least 15 minutes between images. These observations typically last for 300 s, with a typical limiting magnitude of 21.5. ToO observations are typically conducted on the first two nights following a neutrino alert, before swapping to

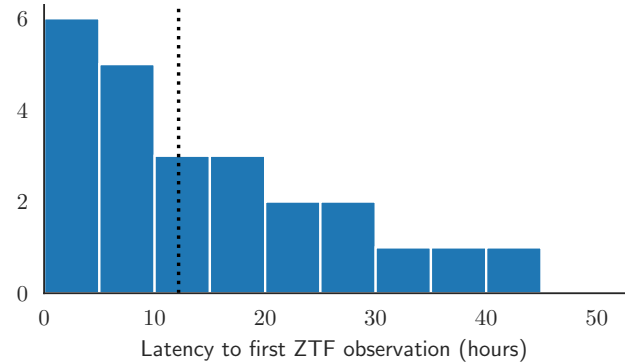


**Figure 1.** Latency between neutrino detection and first ZTF coverage. The median latency time of 12.2 hours is indicated by the vertical dotted line.

serendipitous coverage with shorter 30 s exposures and a 2-day cadence as part of the public survey. As can be seen in Figure 1, our first coverage of events has a median latency of 12.2 hours from neutrino detection. Some latency is unavoidable because the neutrino localisation itself is typically only released with a delay of  $\geq 2$  hours, but additional latency arises primarily due to observability constraints. Poor weather can prevent observations on the first night after neutrino detection, leading to 20% of alerts observed with a latency >24 hours. Serendipitous coverage from the public survey, with a median latency of 24 hours after neutrino detection, reduces the latency for some campaigns.

As for all ZTF data, these observations are first processed by the Infra-red Processing and Analysis Centre (IPAC) to identify detections in difference images (Masci et al. 2019). These detections are then processed by our dedicated data analysis pipeline, *NuZTF* (Stein et al. 2021b), which searches for extragalactic ZTF detections coincident with external triggers. For neutrinos followed-up by ZTF, we define spatial coincidence as requiring that an object lies within the reported 90% localisation rectangle from IceCube, and define temporal coincidence as requiring that an object is detected at least once following the neutrino arrival time.

*NuZTF* is built using the *AMPEL* software framework (Nordin et al. 2019), based on a search algorithm for extragalactic transients. Cuts are applied to reject spurious detections, stars and solar system objects (see Stein et al. 2021a for more details). Searching for detections in the window from neutrino arrival time to 14 days post-neutrino, these cuts typically yield 1 good candidate per  $\sim 3$  sq. deg. of observed sky.

Promising candidates are prioritised for spectroscopic classification, to confirm or rule out a possible association with a given neutrino. Once classified, an object can then be cross-referenced to relevant neutrino emission scenarios for that population. In particular, optical signatures we look for include:

- **Supernovae with evidence of CSM interaction.** High-energy neutrinos are thought to be produced when CCSNe occur within a dense circumstellar medium (CSM), with the resultant shock collisions then generating neutrino emission (Murase et al. 2011). The presence of such CSM interaction also results in characteristic narrow lines in the optical spectrum, so these models generally apply to the Type II<sub>n</sub> supernova population which exhibits these lines. The neutrino emission is expected to be highest close to optical peak, and to then decay over time. In this case, the expected optical signature would be a young Type II<sub>n</sub> supernova close to peak or relatively soon afterwards.

<sup>1</sup> <https://gcn.gsfc.nasa.gov>

Event	R.A. (J2000) [deg]	Dec (J2000) [deg]	90% area [sq. deg.]	ZTF obs [sq. deg.]	Latency [hours]	Signalness	References
IC190503A	120.28	+6.35	1.9	1.4	10.2	36%	<a href="#">Blaufuss (2019c)</a> <a href="#">Stein et al. (2019a)</a>
IC190619A	343.26	+10.73	27.2	21.6	20.9	55%	<a href="#">Blaufuss (2019e)</a> <a href="#">Stein et al. (2019b)</a>
IC190730A	225.79	+10.47	5.4	4.5	7.5	67%	<a href="#">Stein (2019a)</a> <a href="#">Stein et al. (2019c)</a>
IC190922B	5.76	-1.57	4.5	4.1	8.0	51%	<a href="#">Blaufuss (2019h)</a> <a href="#">Stein et al. (2019d)</a>
IC191001A	314.08	+12.94	25.5	23.1	7.4	59%	<a href="#">Stein (2019c)</a> <a href="#">Stein et al. (2019e)</a>
IC200107A	148.18	+35.46	7.6	6.3	2.0	–	<a href="#">Stein (2020a)</a> <a href="#">Stein &amp; Reusch (2020)</a>
IC200109A	164.49	+11.87	22.5	22.4	32.4	77%	<a href="#">Stein (2020b)</a> <a href="#">Reusch &amp; Stein (2020a)</a>
IC200117A	116.24	+29.14	2.9	2.7	22.0	38%	<a href="#">Lagunas Gualda (2020a)</a> <a href="#">Reusch &amp; Stein (2020b)</a> <a href="#">Reusch &amp; Stein (2020c)</a>
IC200512A	295.18	+15.79	9.8	9.3	1.7	32%	<a href="#">Lagunas Gualda (2020c)</a> <a href="#">Reusch et al. (2020a)</a>
IC200530A	255.37	+26.61	25.3	22.0	0.2	59%	<a href="#">Stein (2020e)</a> <a href="#">Reusch et al. (2020b)</a> <a href="#">Reusch et al. (2020c)</a>
IC200620A	162.11	+11.95	1.7	1.2	25.8	32%	<a href="#">Santander (2020b)</a> <a href="#">Reusch et al. (2020e)</a>
IC200916A	109.78	+14.36	4.2	3.6	14.7	32%	<a href="#">Blaufuss (2020e)</a> <a href="#">Reusch et al. (2020f)</a> <a href="#">Reusch et al. (2020g)</a>
IC200926A	96.46	-4.33	1.7	1.3	4.1	44%	<a href="#">Lagunas Gualda (2020g)</a> <a href="#">Reusch et al. (2020h)</a>
IC200929A	29.53	+3.47	1.1	0.9	14.1	47%	<a href="#">Lagunas Gualda (2020h)</a> <a href="#">Weimann et al. (2020a)</a>
IC201007A	265.17	+5.34	0.6	0.6	4.8	88%	<a href="#">Santander (2020c)</a> <a href="#">Reusch et al. (2020i)</a>
IC201021A	260.82	+14.55	6.9	6.3	43.7	30%	<a href="#">Lagunas Gualda (2020i)</a> <a href="#">Stein et al. (2020b)</a>
IC201130A	30.54	-12.10	5.4	4.5	7.1	15%	<a href="#">Lagunas Gualda (2020l)</a> <a href="#">Weimann et al. (2020b)</a>
IC201209A	6.86	-9.25	4.7	3.2	16.9	19%	<a href="#">Lagunas Gualda (2020m)</a> <a href="#">Reusch et al. (2020j)</a>
IC201222A	206.37	+13.44	1.5	1.4	35.2	53%	<a href="#">Blaufuss (2020k)</a> <a href="#">Stein et al. (2020c)</a>
IC210210A	206.06	+4.78	2.8	2.1	0.2	65%	<a href="#">Lagunas Gualda (2021a)</a> <a href="#">Reusch et al. (2021b)</a>
IC210510A	268.42	+3.81	4.0	3.7	5.1	28%	<a href="#">Santander (2021c)</a> <a href="#">Stein et al. (2021c)</a>
IC210629A	340.75	+12.94	6.0	4.6	15.4	35%	<a href="#">Santander (2021f)</a> <a href="#">Necker et al. (2021)</a>
IC210811A	270.79	+25.28	3.2	2.7	26.7	66%	<a href="#">Santander (2021h)</a> <a href="#">Stein et al. (2021d)</a>
IC210922A	60.73	-4.18	1.6	1.2	16.1	92%	<a href="#">Lincetto (2021a)</a> <a href="#">Weimann et al. (2021)</a>

Table 1. Summary of the 24 neutrino alerts followed up by ZTF since survey start on 2018 March 20.

• **Supernovae with relativistic jets.** Some supernovae have been observed to launch relativistic jets as part of the core-collapse process (Galama et al. 1998). Those jets which proceed to escape the surrounding stellar envelope and CSM can be observed as long GRBs if they are oriented towards Earth. Analogously, where an on-axis supernova jet does not escape the stellar envelope, there would instead be a so-called ‘choked jet’ (Nakar 2015). For both scenarios, neutrino emission would primarily be expected during the ‘prompt phase’, in the  $\sim 100$ s after supernova explosion (Waxman & Bahcall 1997; Senno et al. 2016). This scenario would then lead to a young supernova, typically of Type Ic-BL, appearing at the location of the neutrino. The supernova would have an explosion time compatible with the neutrino detection time, and since SNe brighten over a period of days, this optical signature would be delayed relative to the neutrino itself.

• **GRB Afterglows.** Another signature of the supernova jet scenario would be the direct detection of a long-GRB afterglow. Models have also predicted neutrino emission for short GRBs, so a short-GRB afterglow could also be a potential counterpart (Waxman & Bahcall 1997). These GRB afterglows would not be detected before the neutrino detection, and would fade rapidly over the next few hours before falling below the ZTF detection threshold.

• **AGN Flares.** AGN flares, and especially blazar flares, have been suggested as neutrino sources (Bednarek & Protheroe 1999), though the neutrino emission itself would not necessarily be directly correlated to the optical emission. For example, for the standard two-hump Spectral Energy Distribution (SED) model, the optical emission could serve primarily as a tracer for photon target density but not necessarily PeV proton luminosity. We restrict ourselves to searches for AGN undergoing significant optical flaring coincident with a neutrino. Neutrinos could also be produced in AGN without coincident optical flares, but such neutrino emission scenarios are not best probed with an optical follow-up program such as ours.

• **Tidal Disruption Events.** TDEs have been suggested as neutrino sources, through multiple emission channels such as jets, outflows or in coronae (see Hayasaki 2021 for a recent review). The timescale for neutrino production remains unclear, but would not be expected prior to the TDE itself. Non-thermal emission from TDEs can last several hundred days, so the signature in this case would be any ‘ongoing’ TDE coincident with a neutrino.

We do not explicitly reject objects with a history of variability, because variable objects have been proposed as possible neutrino sources. However, our program is intended to identify increased optical flux that is contemporaneous with a neutrino’s detection, so only variable objects with significantly enhanced flux relative to reference images are selected by our pipeline. The blazar flare of TXS 0506+056 fell into this category (IceCube Collaboration et al. 2018), and we would be capable of identifying similar examples.

To date, the *NuZTF* pipeline has identified 172 candidates for visual inspection, out of an observed area of 154.33 sq. deg across 24 neutrinos. This corresponds to an initial density of 1.05 candidates per sq. deg. of sky. The full list of candidates for each neutrino is given in the Appendix.

Visual inspection then enables us to further classify objects and reject background detections. Viewing difference images directly enables us to identify additional image artefacts. We select likely stars through cross-matches to Gaia (Gaia Collaboration et al. 2018),

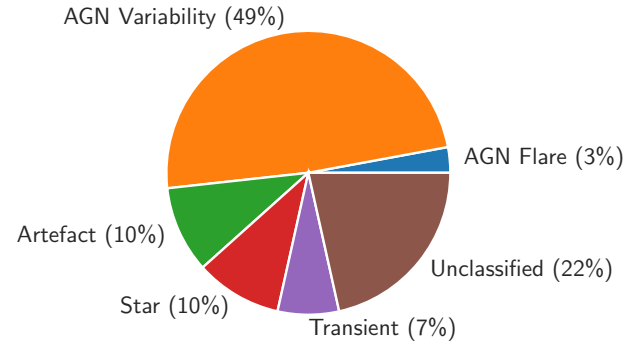


**Figure 2.** Breakdown of the classification of 172 candidates selected by our program for visual inspection.

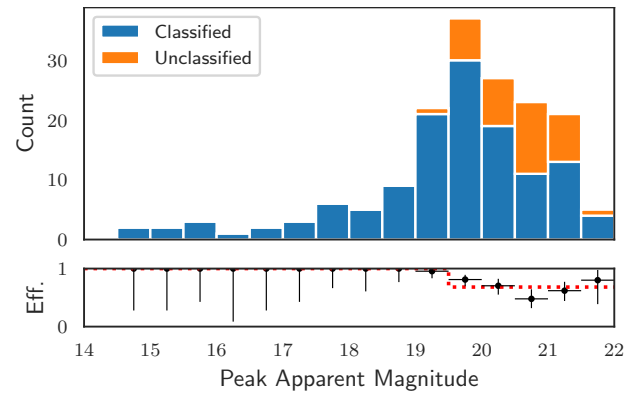


**Figure 3.** Top: Apparent magnitude distribution of candidates selected for visual inspection. Bottom: Classification efficiency as a function of peak apparent magnitude. The red dashed line indicates our step-function approximation of classification efficiency.

where we reject sources with significant ( $3\sigma$ ) evidence for parallax, and to SDSS star/galaxy morphology classifications (Stoughton et al. 2002).

We then flag AGN through matches to catalogued sources in the Milliquas catalogue (Flesch 2021), or via WISE colour cuts (Wright et al. 2010; Stern et al. 2012). We seek to distinguish between ‘routine’ AGN variability and extreme AGN flares. We search for evidence of flaring activity at the time of neutrino detection using the data provided in the ZTF alert packets, which are based on difference images. For cases where a source appears to be significantly variable, or may have been flaring at the time of neutrino detection, we run dedicated forced photometry on the science images to produce a source lightcurve (Masci et al. 2019). We reject AGN with no evidence for contemporaneous flaring as ‘AGN variability’. After removing those sources flagged as stars (17), image artefacts (17) or AGN variability (84), we are left with 54 ‘interesting candidates’. The full breakdown in classification is shown in Figure 2.

These interesting candidates include potential transients, which we seek to classify spectroscopically. Some objects will have already been classified serendipitously, in particular those brighter than 19.0 mag selected by the ZTF Bright Transient Survey (Fremming et al. 2020; Perley et al. 2020). The efficiency with which candidates were classified can be seen in Figure 3. Above a peak apparent magnitude of 19.5, almost all candidates are classified. There were 106 fainter candidates in total, of which 68% were classified. The spectroscopic programs which supported our program are listed in Table 2.

The transients are further broken down by subclass in Figure 4.

Instrument	Semesters
SEDm	2018, 2019, 2020, 2021
NOT	2021B (OPT21B_50, PI: Franckowiak) 2021B (P64-112) 2021B (P61-501) 2022A (22A013, PI: Franckowiak)
TNG	2021B (OPT21B_50, PI: Franckowiak) 2022A (22A01, PI: Franckowiak)
GEMINI	2021A (GN-2021A-Q-116, PI: Kasliwal) 2021B (GN-2021B-Q-117, PI: Kasliwal)
GTC	2020B (GTC73-20B, PI: Amaro Seoane)

**Table 2.** Summary of dedicated spectroscopic programs for our neutrino follow-up program.

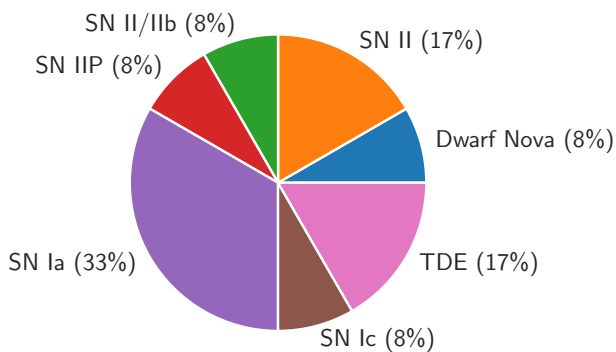


**Figure 4.** Breakdown of the 12 identified transients by subclass.

Four could be immediately excluded as candidates based on their classification as SNe Ia, a population not predicted to emit neutrinos. Of the remainder, beyond the two TDEs, no further sources exhibited electromagnetic signatures consistent with the neutrino emission scenarios listed above.

A selection of highlighted results is given in the following sections. ZTF data for three other candidate neutrino sources from the literature, PKS 1502+106, BZB J0955+3551 and PKS 0735+178 are also outlined in Section 5. We omit ZTF data for the probable neutrino-TDEs AT2019dsg and AT2019fdr, as these have already been released in dedicated publications (Stein et al. 2021a; Reusch et al. 2021a).

### 3 CANDIDATE TRANSIENT COUNTERPARTS

#### 3.1 SN 2019pqh and IC190922B

Follow-up of IC190922B by ZTF identified the candidate supernova SN 2019pqh/ZTF19abxtupj (Stein et al. 2019d). The lightcurve is shown in Figure 5, where upper limits are illustrated with triangles. The arrival time of the neutrino on 2019 September 22 is marked with a dotted line, and the supernova is detected in the subsequent ToO observations. The neutrino arrival time was close to optical peak, consistent with a CSM-interaction scenario.

However, a spectrum was taken by the *NUTS2 collaboration* (Holmbo et al. 2019), and the supernova was classified as a Type II supernova without spectroscopic signatures of CSM interaction (Reguitti et al. 2019). A higher-resolution spectrum of the object

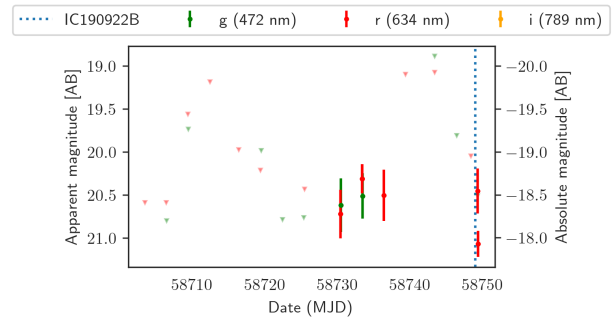


**Figure 5.** ZTF lightcurve of SN 2019pqh. The arrival time of neutrino IC190922B is marked by the dashed blue line.

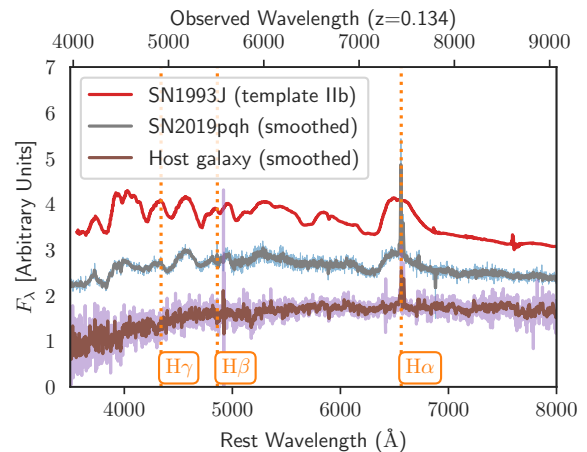


**Figure 6.** Spectrum of SN2019pqh, taken on 2019 September 28. A historical spectrum of the host galaxy taken by SDSS, and a similar spectrum of a Type IIb supernova, are provided for comparison.

was also obtained on 2019 September 28, shown in Figure 6, using the *Low Resolution Imaging Spectrometer* (LRIS) spectrograph at the Keck observatory (PI: Kasliwal?) (Oke et al. 1995). A historical spectrum of the host galaxy, taken by the *Sloan Digital Sky Survey* (SDSS; Abolfathi et al. (2018)), is also shown in Figure 6. Both the transient and host galaxy exhibit prominent Balmer lines, highlighted in orange in Figure 6, from which a redshift of 0.134 is derived. A template-matching classification using SNID (Blondin & Tonry 2007) yields a match to a Type IIb supernova (SN 1993J, Barbon et al. 1995) 2 days before peak, also shown in Figure 6.

With this redshift, a peak absolute magnitude of  $-18.6$  was derived, atypically bright for such a Type IIb supernova (see e.g. Lyman et al. 2016). One explanation for this enhanced luminosity could be CSM interaction, through which additional kinetic energy is converted to electromagnetic emission. However, the lack of corresponding narrow line spectroscopic signatures generally disfavours the existence of CSM-interaction, and thus any associated neutrino emission from this object. It is therefore likely that SN 2019pqh is instead unrelated to the neutrino IC190922B.

#### 3.2 SN 2020lam and IC200530A

ZTF serendipitously observed the localisation of neutrino alert IC200530A just 10 minutes after detection (Stein 2020e), as part of routine survey operations (Reusch et al. 2020b). Additional ToO

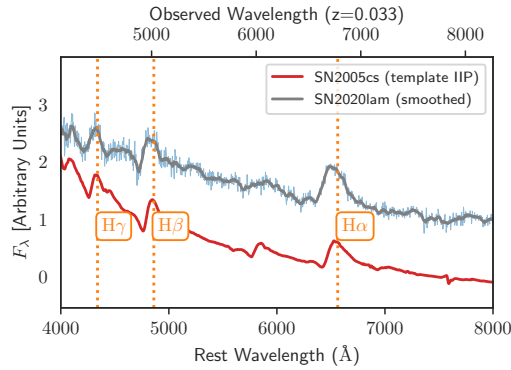


**Figure 7.** Spectrum of SN2020lam, taken on 2020 June 6. A similar spectrum, from Type IIP supernova SN 2005cs, is shown for comparison.

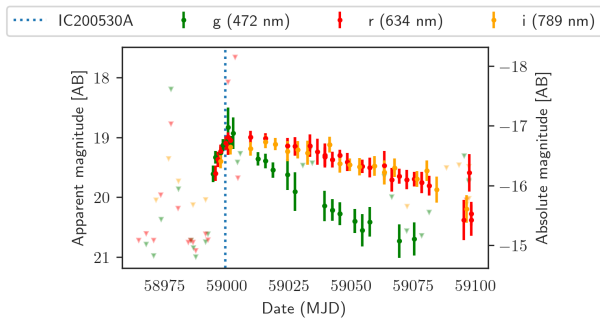


**Figure 8.** ZTF lightcurve of SN2020lam. The arrival time of neutrino IC200530A is marked by the dashed blue line.

observations were then conducted on 2020 May 31 in *g* and *r* band, and again on 2020 June 1. During ZTF follow-up of IC200530A, SN 2020lam/ZTF20abbpkpa was identified as a candidate supernova and potential optical counterpart (Reusch et al. 2020b). Spectroscopic observations were triggered using the NOT/ALFOSC spectrograph on 2020 June 6 (PI: Sollerman), which confirmed SN2020lam as a Type II supernova using SNID (Reusch et al. 2020c). This spectrum is shown in Figure 7, alongside the matching Type IIP supernova (SN 2005cs, Pastorello et al. 2006) mapped to the same redshift.

As seen in the lightcurve in Figure 8, the supernova was close to peak at neutrino detection time. The object then rapidly cooled, and thus reddened, as is typical for supernovae. Given the neutrino arrival time, CSM-interaction would be the only viable neutrino production mechanism. However, the spectrum shown in Figure 7 had no narrow lines, and therefore did not provide any evidence supporting such CSM interaction. SN 2020lam was therefore likely unrelated to IC200530A.

### 3.3 SN 2020lls and IC200530A

SN 2020lls/ZTF20abndpdo was also identified as a candidate supernova during ZTF follow-up of IC200530A, (Reusch et al. 2020b). Spectroscopic observations were again triggered using the NOT/ALFOSC spectrograph on 2020 June 12 (PI: Sollerman), which confirmed that SN 2020lls was a Type Ic supernova without broad-line features (Reusch et al. 2020d). This spectrum is illustrated in Figure 9, alongside a matching Type Ic supernova spectrum from SNID mapped to the same redshift (Taubenberger et al. 2006). Given that the supernova had not been detected in alert data prior to the

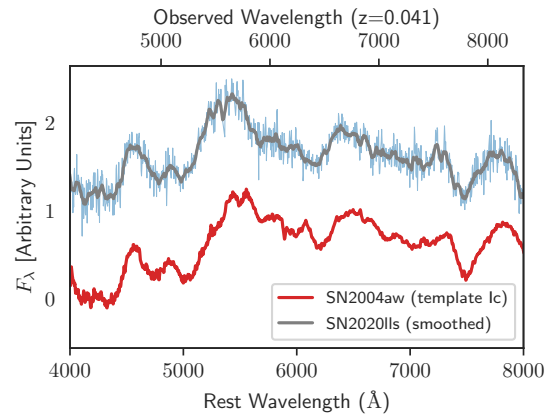


**Figure 9.** Spectrum of SN 2019lls, taken on 2020 June 13. A similar spectrum, of Type Ic supernova SN 2004aw, is shown for comparison.

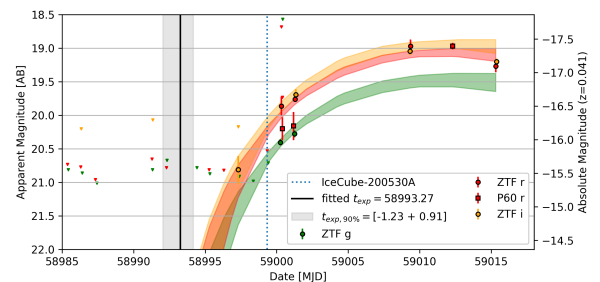


**Figure 10.** ZTF lightcurve of SN2020lls. The arrival time of neutrino IC200530A is marked with the blue dotted line. The supernova model fit from *MOSFIT* is indicated by the shaded orange/red/green bands, and the the best-fit explosion time is given by the vertical black line.

neutrino arrival time, and that it belonged to the subpopulation associated with relativistic jets, SN 2020lls was a candidate for the choked-jet neutrino production model.

However, as can be seen in Figure 10, forced photometry analysis (Reusch 2020) revealed a lower-threshold *i*-band ZTF detection preceding the neutrino arrival. Additionally, modelling of the lightcurve using the *MOSFIT* software (Guillochon et al. 2018) revealed an estimated explosion date predating the neutrino by a week. In combination, these results disfavoured any supernova explosion origin for the neutrino, suggesting that SN 2020lls was instead unrelated to IC200530A (Reusch et al. 2020d).

## 4 AGN FLARE CANDIDATES

While the vast majority of AGN detections from our pipeline were categorised as ‘AGN variability’, visual inspection revealed five AGN which appeared to possibly undergo optical flaring at the time of neutrino detection. The forced photometry lightcurves of these five flares are shown in Figure 11. We attempt to quantify whether the optical lightcurves of these AGN identify them as candidate neutrino sources.

We can consider possible optical signatures associated with neutrino emission. One scenario is the optical flaring observed for TXS 0506+056 during the detection of neutrino IC170922A (IceCube Collaboration et al. 2018). In particular, the optical apparent V-band

329 magnitude of TXS 0506+056 was observed to increase from 15.0 to  
 330 14.5 during the time of neutrino detection, corresponding to a flux in-  
 331 crease of >50%, over a period of 50 days, relative to the pre-neutrino  
 332 baseline.

333 AGN can also exhibit short-term variability for periods of hours or  
 334 days, but we caution that the detection of a high-energy neutrino alert  
 335 is a process that requires a substantial fluence at the IceCube detector,  
 336 even after accounting for the significant Eddington bias associated  
 337 with cosmic neutrino detection (Strotjohann et al. 2019). The cor-  
 338 responding neutrino flux that is required is inversely proportional to the  
 339 duration of neutrino emission, and therefore associating a neutrino  
 340 detection with a temporary electromagnetic signature lasting hours  
 341 or days would imply an extremely high average neutrino flux for the  
 342 duration of that signature. Such highly luminous rapid neutrino flares  
 343 are not well motivated theoretically, it is therefore unlikely that short  
 344 AGN flares are indicators of neutrino production.

345 In contrast, longer-term electromagnetic signatures can serve as  
 346 tracers for neutrino emission. For example, month-long flaring peri-  
 347 ods of substantially elevated flux can dominate the neutrino emission  
 348 of blazars (see e.g. Rodrigues et al. 2021). Very long flares, with du-  
 349 rations of years, could also be relevant for neutrino production. How-  
 350 ever, given the relatively short baseline of ZTF observations, our  
 351 neutrino follow-up program is not well-suited to identify them. We  
 352 therefore restrict ourselves to searching for such month-long optical  
 353 flares, as was observed for TXS 0506+056.

354 We calculate the median flux for each of the five AGN, and each  
 355 ZTF filter, in a  $\pm 25$  day window centered on the neutrino detection.  
 356 We divide this instantaneous flux by the median flux of the source  
 357 in that filter over the entire  $\sim 4$  year ZTF baseline, giving a proxy  
 358 for relative optical flare strength. These values are given in Table  
 359 3. Of the five AGN, only one (ZTF18aavccmo, upper panel of Fig-  
 360 ure 11) had a median instantaneous flux >50% above the baseline  
 361 median flux. ZTF18aavccmo reached this threshold in both g and r  
 362 band. We conclude that the remaining four AGN (ZTF18abrwqpr,  
 363 ZTF20aamoxyt, ZTF18abxrpgu, ZTF19aasfvqm) do not exhibit sub-  
 364 stantial neutrino-coincident optical flares, and we therefore find no  
 365 evidence to suggest they are counterparts to high-energy neutrinos.

366 ZTF18aavccmo, cross-matched to source WISEA  
 367 J170539.32+273641.2, is classified as a likely QSO in the  
 368 Milliquas catalogue. It underwent a single coherent flare lasting  
 369 approximately one year, with a peak flux roughly triple the quiescent  
 370 flux measured by ZTF. It was coincident with neutrino IC200530A,  
 371 detected during the decay of the optical flare. However, this flare was  
 372 extremely faint, with a median flux at the time of neutrino detection  
 373 was  $\nu F_\nu \approx 5 \times 10^{-13}$  erg cm $^{-2}$  s $^{-1}$ . This is a factor of 20 lower  
 374 than the flux observed for TXS 0506+056 during the detection of  
 375 IC170922A (IceCube Collaboration et al. 2018). We thus identify  
 376 no optical AGN flares which resemble the multi-wavelength flare  
 377 of TXS 0506+056 in 2017, from any of our 24 neutrino follow-up  
 378 campaigns.

379 While our results do not preclude a significant degree of neutrino  
 380 emission from AGN more broadly, they disfavour scenarios where the  
 381 vast majority of astrophysical neutrinos are produced by bright AGN  
 382 optical flares. There is no tension with scenarios where AGN neutrino  
 383 emission is not dominated by bright optical flares, for example the  
 384 ‘steady state’ AGN neutrino models tested in Abbasi et al. (2021) or  
 385 scenarios where AGN neutrino emission is correlated only to gamma-  
 386 ray flares. A more systematic study of correlations between ZTF-  
 387 detected AGN flares and neutrinos, including calculations of chance  
 388 coincidence probabilities, will be the subject of a future analysis.

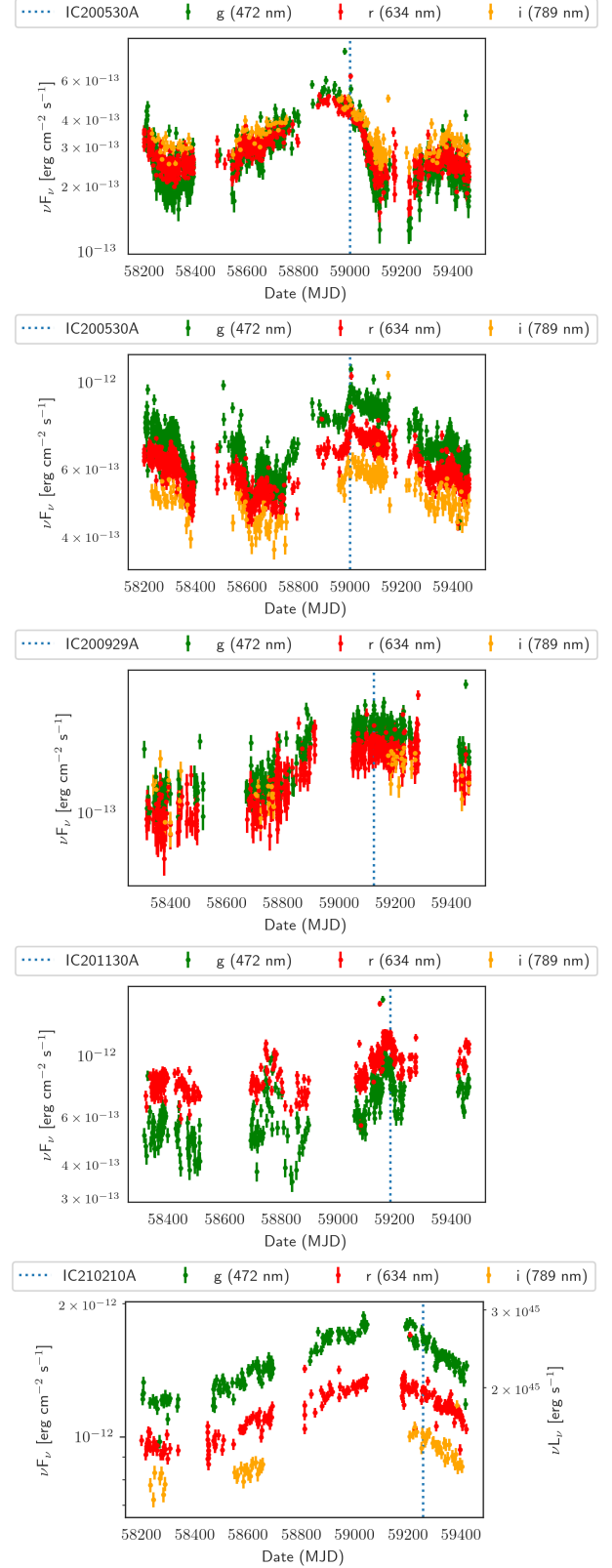


**Figure 11.** ZTF lightcurve of 5 AGN flares coincident with high-energy neutrinos. From top to bottom, the sources are: ZTF18aavccmo, ZTF18abrwqpr, ZTF20aamoxyt, ZTF18abxrpgu, ZTF19aasfvqm.

Object	Filter	Inst. Flux [ $10^{-13}$ erg cm $^{-2}$ s $^{-1}$ ]	Med. flux [ $10^{-13}$ erg cm $^{-2}$ s $^{-1}$ ]	Inst. Flux / Med. flux
ZTF18aavecmo	g	4.7	2.6	1.83
ZTF18aavecmo	r	4.3	2.6	1.65
ZTF18aavecmo	i	4.5	3.1	1.44
ZTF18abrwqpr	g	9.0	6.9	1.31
ZTF18abrwqpr	r	7.4	5.8	1.27
ZTF18abrwqpr	i	6.0	5.3	1.14
ZTF20aamoxyt	g	3.1	2.5	1.24
ZTF20aamoxyt	r	2.4	1.7	1.43
ZTF18abxrpgu	g	8.8	6.5	1.37
ZTF18abxrpgu	r	11.2	8.7	1.28
ZTF19aasfvqm	g	16.5	14.8	1.12
ZTF19aasfvqm	r	12.7	11.6	1.09
ZTF19aasfvqm	i	10.0	8.9	1.13

**Table 3.** Summary of the 5 AGN flares coincident with neutrinos, including the instantaneous flux during neutrino detection, median flux over the entire ZTF baseline, and the ratio of these values.

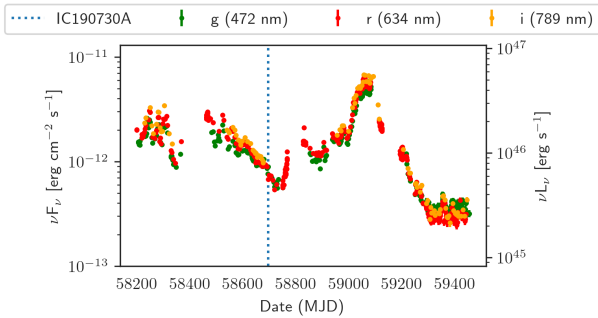


**Figure 12.** ZTF lightcurve of blazar PKS 1502+106. The arrival time of neutrino IC190730A is marked with the vertical dashed line.

## 5 CANDIDATE NEUTRINO SOURCES FROM THE LITERATURE

We here provide data on various candidate neutrino sources reported in the literature. However, we caution that none of the objects presented here were selected by our pipeline as ZTF candidates, and therefore are not considered part of our systematic search for neutrino counterparts. We would not claim any such object as a candidate neutrino sources in our neutrino follow-up program, because the chance coincidence probability would be unquantifiable. Any search for additional candidate neutrino sources, beyond those candidates found by our pipeline following ToO observations, would require an independent and unbiased systematic analysis procedure.

### 5.1 PKS 1502+106

The neutrino IC190730A was reported by IceCube in spatial coincidence with PKS 1502+106, a particularly gamma-bright Flat Spectrum Radio Quasar (FSRQ) (Stein 2019a). The object was observed by ZTF as part of ToO observations, and was detected under the ZTF candidate name ZTF18aaqnqzx (Stein et al. 2019c). The blazar had already been repeatedly detected as part of the routine survey operations, with both positive and negative flux changes relative to survey reference images.

The blazar lightcurve is shown in Figure 12, using data from sci-

ence images with the ZTF forced photometry service (Masci et al. 2019). The neutrino arrival time is marked in blue. There was no significant flaring observed for this source coincident with the neutrino. The blazar at this point was dimmer than survey reference images, with the neutrino arriving during a year-long fading, and consequently was not selected by our follow-up pipeline as a possible counterpart. There is thus no evidence from the contemporaneous ZTF data to suggest a causal connection between IC190730A and PKS 1502+106, consistent with data from other observatories which did not see any evidence of short-term flaring (Franckowiak et al. 2020).

Data from the Owens Valley Radio Observatory (OVRO) did reveal that the radio flux was elevated in the months preceding the neutrino detection relative to the decade-long observation baseline, behaviour which has also been claimed for TXS 0506+056 and other neutrino-coincident blazars (Kiehlmann et al. 2019). Comprehensive time-dependent modelling has found that the detection of a neutrino alert from PKS 1502+106 is consistent with the multi-wavelength observations of this object, so a neutrino-blazar association is plausible but likely unrelated to the flaring activity (Rodrigues et al. 2021). In any case, the new optical data presented here can be used to further constrain such neutrino emission scenarios.

### 5.2 BZB J0955+3551

IC200107A was a high-energy neutrino reported by IceCube (Stein 2020a) which was later identified to be in spatial and temporal coincidence with a blazar undergoing a dramatic simultaneous X-ray flare (Krauss et al. 2020; Giommi et al. 2020c). The source BZB J0955+3551 (also known as 4FGL J0955.1+3551 and 3HSP J095507.9+355101) belongs to the specific subclass of extreme blazars, which are characterised by synchrotron peaks at very high frequencies, which had been proposed as especially promising candidates of high-energy neutrinos (Padovani et al. 2016).

More comprehensive multi-frequency modelling has confirmed that the detection of a neutrino alert from an extreme blazar is plausible, though the simultaneous X-ray flare may not be directly related to the neutrino production (Paliya et al. 2020; Giommi et al. 2020b; Petropoulou et al. 2020). The ZTF lightcurve for BZB J0955+3551



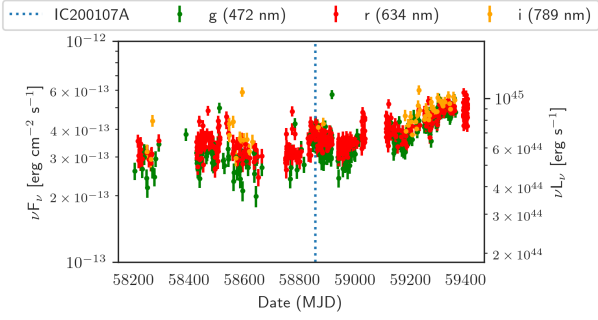


**Figure 13.** ZTF lightcurve of blazar BZB J0955+3551. The arrival time of neutrino IC200107A is marked with the vertical dashed line.

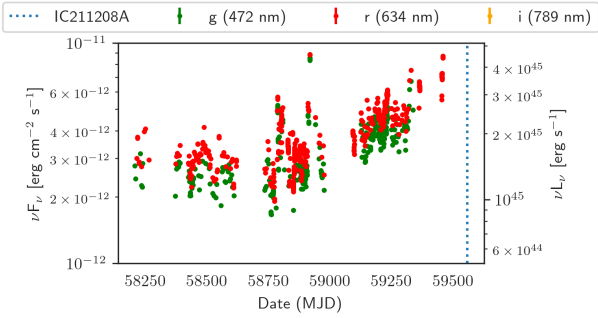


**Figure 14.** ZTF lightcurve of blazar PKS 0735+178. The arrival time of neutrino IC211208A is marked with the vertical dashed line.

is shown in Figure 13. There is no evidence of any optical flaring on short or long timescales coincident with the detection of IC200107A.

### 5.3 PKS 0735+178

The neutrino IC211208A was reported by IceCube with an estimated 50% signalness (Santander 2021k). ZTF was down for maintenance during the arrival of IC211208A, and therefore we did not trigger ToO follow-up observations. However, MASTER reported the detection of the brightened blazar PKS 0735+178 during their follow-up of this alert (Zhirkov et al. 2021). The blazar had already been reported as being in a bright state one month prior (Savchenko et al. 2021). Observations by Fermi-LAT confirmed that the blazar was also flaring in gamma rays, but it was noted that the source lay outside the 90% localisation reported by IceCube (Garrappa et al. 2021a). Similar flaring was also reported in radio (Kadler et al. 2021b) and X-rays (Santander & Buson 2021).

We here share our ZTF data for this source, shown in Figure 14. Although we have no data at the neutrino arrival time, we confirm the months-long optical brightening preceding the detection of IC211208A reported by Savchenko et al. (2021). This object would meet our definition of an optical AGN flare rather than variability, based on visual inspection of the lightcurve.

We note however that, even if ZTF had been able to observe the neutrino, this source would not have been selected by our pipeline because it was outside the 90% localisation reported by IceCube. A clear and consistent definition of spatial coincidence is an essential component of our program, because it is a prerequisite to appropriately account for the impact of the ‘look-elsewhere’ effect for any counterparts that are identified. However, as a consequence of our criteria, the ~10% of neutrino sources which lie outside their respec-

Event	$P_{\text{astro}}$	$P_{\text{obs}}$	$P_{\text{astro}} \times P_{\text{obs}}$
IC190503A	0.36	0.64	0.23
IC190619A	0.55	0.71	0.39
IC190730A	0.67	0.75	0.50
IC190922B	0.51	0.82	0.42
IC191001A	0.59	0.81	0.48
IC200107A	0.50	0.74	0.37
IC200109A	0.77	0.89	0.69
IC200117A	0.38	0.84	0.32
IC200512A	0.32	0.85	0.27
IC200530A	0.59	0.78	0.46
IC200620A	0.32	0.65	0.21
IC200916A	0.32	0.77	0.25
IC200926A	0.44	0.66	0.29
IC200929A	0.47	0.70	0.33
IC201007A	0.88	0.87	0.77
IC201021A	0.30	0.82	0.25
IC201130A	0.15	0.75	0.11
IC201209A	0.19	0.61	0.12
IC201222A	0.53	0.82	0.43
IC210210A	0.65	0.67	0.43
IC210510A	0.28	0.82	0.23
IC210629A	0.35	0.69	0.24
IC210811A	0.66	0.76	0.50
IC210922A	0.93	0.67	0.62

**Table 4.** Probability of finding a counterpart for each neutrino, assuming counterparts are sufficiently bright to be detected by our ZTF neutrino follow-up program.

tive 90% probability contours will by definition not be identified by our program.

## 6 LIMITS ON NEUTRINO SOURCE POPULATIONS

With our program, we did not find any likely candidate counterparts from any population except TDEs. We can consider limits that can be placed on other potential sources of astrophysical neutrinos given the non-detections. These limits will clearly not apply for TDEs, because for this population probable counterparts were detected.

For each neutrino, we can consider the probability that an astrophysical counterpart would be detected. A counterpart could only be detected if a given IceCube neutrino was astrophysical, with this as  $P_{\text{astro}}$  probability being reported by IceCube in GCN notices as the ‘signalness’ parameter. For each neutrino that was indeed astrophysical, the source could only then be detected if it lay within the area observed by ZTF. We can estimate this probability,  $P_{\text{obs}}$ , by assuming that the 90% probability is uniformly distributed across the rectangle reported by IceCube,  $A_{\text{IC}}$ , such that:

$$P_{\text{obs}} = 0.9 \times \frac{A_{\text{ZTF}}}{A_{\text{IC}}} \quad (1)$$

where  $A_{\text{ZTF}}$  is the area observed by ZTF after accounting for detector chip gaps.

The probability to find an optical counterpart is then given by the joint probability that the neutrino is astrophysical,  $P_{\text{astro}}$ , that the astrophysical source lay in the observed ZTF area,  $P_{\text{obs}}$ , and the probability that a given counterpart would be detectable with our program  $P_{\text{detectable}}$ . The values of  $P_{\text{astro}}$  and  $P_{\text{obs}}$  for each alert are given in Table 4.

The detectable probability will depend on the selection efficiency,

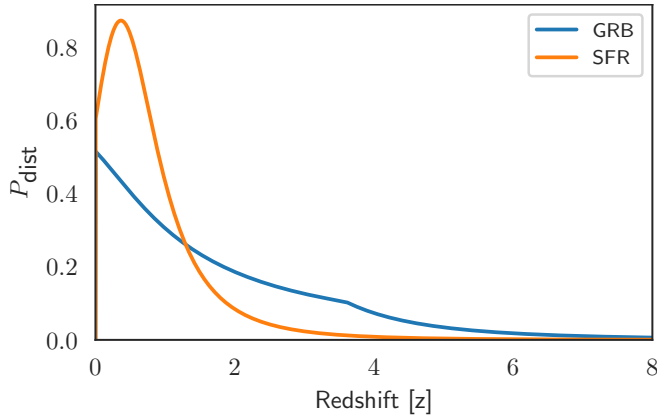


**Figure 15.** PDF for neutrino sources as a function of redshift, for both GRB-like and SFR-like source evolutions.

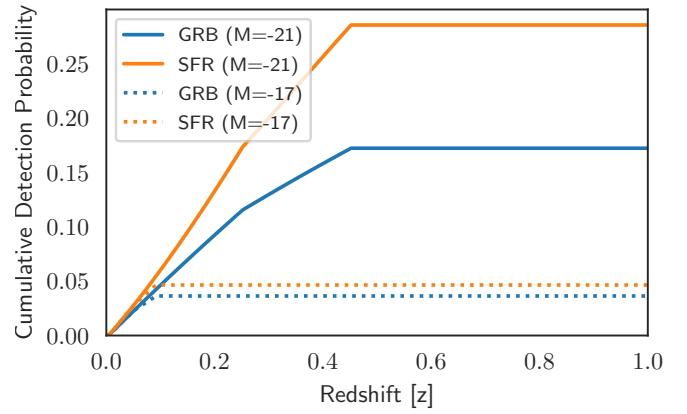


**Figure 16.** Cumulative counterpart detection probability as a function of redshift.

503  $\epsilon_{\text{det}}$ , of our program. This selection efficiency in turn depends on the 533  
 504 apparent magnitude of the electromagnetic counterpart. Motivated by 534  
 505 our classification efficiency in Figure 3, we assume completeness for 535  
 506 objects brighter than 19.5 mag, and a classification efficiency of 68% 536  
 507 for objects fainter than this (this assumption is illustrated with the 537  
 508 red dashed line in Figure 3). We additionally assume a conservative 538  
 509 95% detection efficiency for sources to be found by our pipeline, if 539  
 510 said source was imaged by the camera. Chip gaps in the detector are 540  
 511 already accounted for in Equation 1. Because the detection efficiency 541  
 512 will decrease as the objects approach the ZTF limiting magnitude of 542  
 513 21.5 for 300s exposures, we neglect objects fainter than 21 mag in 543  
 514 our calculation:

$$\epsilon_{\text{selection}}(m) = 0.95 \times \begin{cases} 1.00 & m \leq 19.5 \\ 0.68 & 19.5 \leq m \leq 21.0 \\ 0.00 & 21.0 \leq m \end{cases} \quad (2)$$

515 The fraction of astrophysical neutrino sources that are detected by 547  
 516 our program will depend on the properties of a given population. 548  
 517 For a power law neutrino spectrum, the neutrino flux at Earth for a 549  
 518 transient population as a function of redshift is proportional to:

$$\frac{dF(z)}{dz} \propto \left[ (1+z)^{2-\gamma} \times \frac{R(z)}{4\pi D_L^2} \right] \frac{dV_C}{dz} \quad (3)$$

519 where  $\gamma$  is the intrinsic neutrino spectral index and  $R(z) = \rho(z)/\rho(0)$  550  
 520 is the normalised source redshift evolution for a population with rate 551  
 521  $\rho(z)$ . The neutrino flux scaling is thus independent of the local rate 552  
 522  $\rho(0)$  for a given transient population. By normalising Equation 3, 553  
 523 we can derive a probability density function (PDF) for the redshift 554  
 524 of detected neutrinos:

$$P_{\text{dist}}(z) = \frac{dF(z)}{dz} \left/ \left( \int_0^\infty \frac{dF(z)}{dz} dz \right) \right. \quad (4)$$

525 PDFs for  $P_{\text{dist}}(z)$ , calculated using the *flarestack* code (Stein et al. 558  
 526 2020a), are shown in Figure 15 for redshift evolutions from a ‘GRB- 559  
 527 like’ population (Lien et al. 2014) and from a Star-Formation-Rate 560  
 528 population (‘SFR-like’) (Strolger et al. 2015). It can be seen in Figure 561  
 529 15 that GRB-like populations tend to be at greater distances than 562  
 530 SFR-like ones, with GRB-like neutrinos being emitted from a median 563  
 531 redshift of  $z = 1.34$ , whereas SFR-like neutrinos would have a median 564  
 532 distance of  $z = 0.64$ . This has a direct impact on the population 565

properties compatible with our limits, because a neutrino population 533  
 534 dominated by nearby sources will produce counterparts with brighter 535  
 536 apparent magnitudes.

For a given source evolution, the probability of detecting a coun- 537  
 538 terpart will then ultimately depend on the underlying luminosity 539  
 540 function of the population. For an absolute magnitude,  $M$ , the coun- 541  
 542 terpart detection probability is equal to the integrated product of 543  
 544 the probability that a counterpart has a given redshift,  $P_{\text{dist}}(z)$ , and 545  
 546 the detection efficiency of our program for the apparent magnitude, 547  
 548  $m(M, z)$ , corresponding to that redshift:

$$P_{\text{detectable}}(M) = \int_0^\infty [\epsilon_{\text{det}}(m(M, z)) \times P_{\text{dist}}(z)] dz \quad (5)$$

549 The impact of different evolutions and absolute magnitudes can be 550  
 551 seen in Figure 16. For an absolute magnitude of  $-21$ , our program 552  
 553 would be sensitive to counterparts up to a redshift of  $z \approx 0.45$ , beyond 554  
 555 which  $m > 21$  so  $\epsilon_{\text{selection}} = 0$ . For an SFR-like evolution, this would 556  
 557 correspond to  $P_{\text{detectable}}(-21) = 26\%$ , but for the higher- $z$  GRB-like 558  
 559 neutrino distribution, we would instead find  $P_{\text{detectable}} = 16\%$ . For a 560  
 561 fainter absolute magnitude of  $-17$ , our program would probe a much 562  
 563 smaller volume up to redshift  $z \approx 0.1$ , so then  $P_{\text{detectable}}$  would be 564  
 565 5% and 4% for SFR-like and GRB-like populations respectively.

Combining these values, the joint probability for us to find a coun- 566  
 567 terpart during a follow-up campaign is given by:

$$P_{\text{find}}(f, M) = P_{\text{astro}} \times P_{\text{obs}} \times P_{\text{detectable}}(M) \times f(M) \quad (6)$$

where  $f$  is the fraction of astrophysical neutrino sources with an 568  
 569 absolute magnitude equal to or brighter than  $M$ . The probability that 570  
 571 no counterpart was detected in any of our 24 follow-up observations 572  
 573 is then given by:

$$P_{\text{no\_counterpart}}(M, f) = \prod_{i=1}^{24} (1 - P_{\text{find}, i}(M, f)) \quad (7)$$

574 The probability of no counterpart detection is given in Figure 17 as 575  
 576 a function of  $M$ . The results of our program strongly disfavour scenar- 577  
 578 ios where all neutrino sources have bright absolute magnitudes. The 578  
 579 horizontal dashed line in Figure 17 represents a 10% chance of non- 579  
 580 detection, and thus a 90% confidence limit. We can use this threshold 580  
 581 to set a limit on the luminosity function of neutrino sources, by choos- 581  
 582 ing the appropriate fraction  $f$  such that  $P_{\text{no\_counterpart}}(M, f) > 0.1$  582

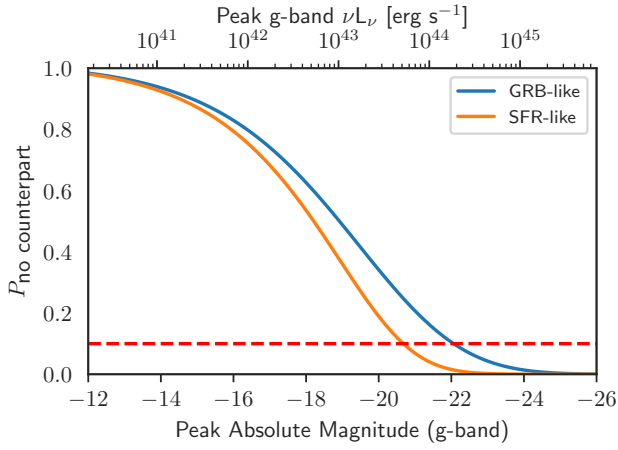


**Figure 17.** Probability of detecting no counterpart as a function of absolute magnitude, assuming  $f=1$ . The dotted line corresponds to 90% confidence.

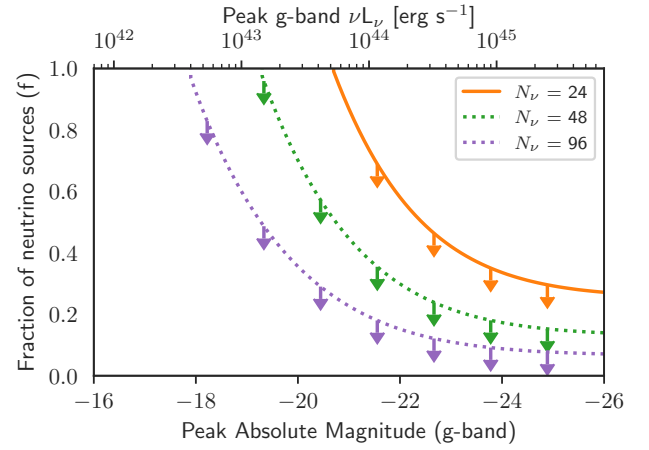


**Figure 19.** Upper limits (90% CL) on the luminosity function of neutrino sources for an SFR-like evolution that would be derived for a ZTF neutrino sample that was twice ( $N_\nu=48$ ) or four times ( $N_\nu=96$ ) the size of the sample presented here.

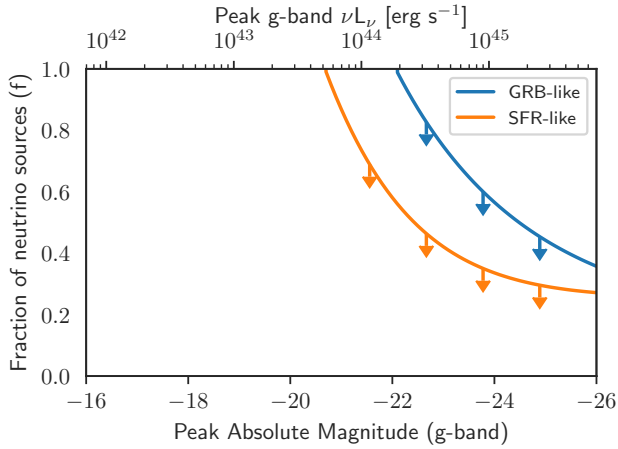


**Figure 18.** Upper limits (90% CL) on the luminosity function of neutrino sources.

These constraints on  $f(M)$  at 90% CL are illustrated in Figure 18, for the two source evolutions. These are generic constraints on the underlying luminosity function of neutrino sources, and are agnostic to the actual nature of the neutrino sources which follow the redshift evolutions. They constrain the aggregate neutrino flux emitted by e.g. a SFR-like population, and thus apply equally well to a composite neutrino flux with e.g. multiple SFR-like neutrino populations. To the best knowledge of the authors, this is the first time generic constraints on the neutrino luminosity function have been derived, though a similar procedure has already been used to derive limits from optical searches for counterparts to gravitational waves (Kasliwal et al. 2020). One novel consequence of these general limits are the first observational constraints on the contribution of the brightest superluminous supernova to the diffuse neutrino flux. Objects brighter than  $-22$  mag can contribute no more than 58% of the total astrophysical neutrino alerts if SFR-like.

It should be noted that these limits assume that a given transient could pass our selection criteria outlined in Section 2, and therefore do not apply to extremely rapid transients such as GRB afterglows, which peak and fade on timescales  $\lesssim 1$  day. Such objects are not well captured by the ZTF public survey cadence or our typical neutrino follow-up observation cadence, and are unlikely to be detected multiple times in order to pass our selection criteria, so our detection efficiency will be somewhat lower.

## 7 CONCLUSIONS

The ZTF neutrino follow-up program coincided with the introduction of the upgraded IceCube alert selection, yielding one unretracted alert every 2 weeks and one ZTF follow-up campaign every 4 weeks on average. The program resulted in the identification of two probable neutrino sources (Stein et al. 2021a; Reusch et al. 2021a), and in the first limits on the optical luminosity function of neutrino sources.

Though the limits presented here constrain only the very brightest transients such as superluminous supernovae, they will continue to become more stringent over time if no new counterparts are identified. As can be seen in Figure 19, extrapolating our analysis to a neutrino sample that was twice or four times as large would lead to substantially more constraining limits, and will be achieved on the present trajectory with 2 or 6 additional years of observations.

Although the data analysis presented considered candidates detected up to 14 days after neutrino detection, our early real-time counterpart searches generally focussed on counterparts detected in the ToO observations scheduled for the first two nights after neutrino detection. Motivated by the systematic analysis performed here, and to improve sensitivity to time-delayed optical signatures such as neutrino emission from choked jets, we have modified our ToO observation strategy to better cover a range of transient timescales. We now trigger deep 300s in  $g$  and  $r$  band on the first night of observations to obtain deep upper limits or faint detections, and to additionally yield colour information for any active transient. However, we replaced our second pair of 300s exposures with a series of 30s exposures spread over subsequent nights, to complement the public survey and ensure good coverage of the photometric evolution of candidates. Forced photometry is only possible for images from the public survey after they have been published as part of the regular ZTF Data Releases, but with this ToO monitoring we can perform forced photometry analysis in real time (Reusch 2020). We can also better prioritise spectroscopic follow-up with photometric classification.

One shortcoming of the ZTF program thus far has been the relatively poor sensitivity to very rapid transients such as GRB afterglows, owing to the median latency of 12.8 hours to first coverage. We plan to implement automated triggering with ZTF, similar to that operated by other observatories such as ASAS-SN (Necker et al. 2022), enabling low-latency observations for at least some favourable neutrino alerts with appropriate accessibility. Dedicated analysis of

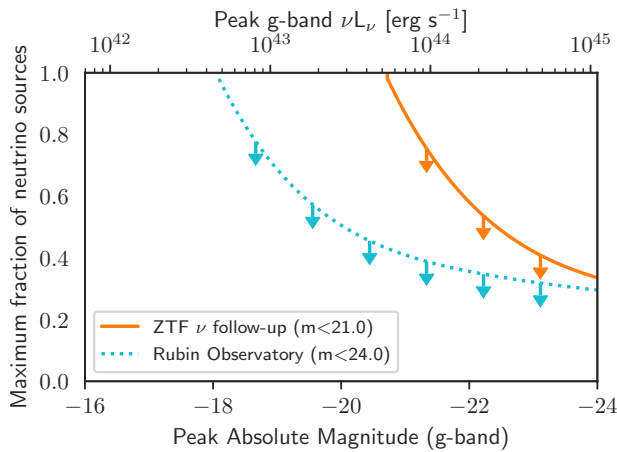


**Figure 20.** Upper limits (90% CL) on the luminosity function for an SFR-like population with our sample of 24 observed neutrino alert and our classification efficiency (ZTF  $\nu$  follow-up), and limits that would be obtained for a comparable neutrino follow-up program with the upcoming Rubin Observatory.

low-latency follow-up campaigns would yield more stringent constraints on GRB afterglows as neutrino sources.

The results and analysis presented here can serve as a pathfinder for future triggered neutrino follow-up programs with wide-field instruments. In particular, ToO observations with the upcoming Vera C. Rubin Observatory would offer an unprecedented opportunity to probe neutrino sources to much higher redshifts (Ivezić et al. 2019). Multi-band observation coverage would enable photometric classification of many candidates, substantially extending the classification efficiency presented in Figure 3 to much greater depths. An illustration of this is presented in Figure 20, assuming that the same neutrino sample in Table 1 had instead been observed with the Rubin Observatory. For a comparable 60% classification efficiency down to 24th mag, the corresponding limits on the neutrino luminosity function would be much more constraining for lower magnitudes. However, for very luminous neutrino sources, the performance of both surveys for such a neutrino sample would be comparable. Given that there are only expected to be  $\sim 12$  astrophysical neutrinos in our sample, observations will never be able to overcome the 90% limit from Poisson counting statistics even if they had a perfect 100% efficiency. Instead, as seen in Figure 19, only larger neutrino samples can enable stricter limits on bright sources.

Beyond optical observatories, similar electromagnetic neutrino follow-up programs are planned for example at near infra-red (NIR) wavelengths with WINTER (Lourie et al. 2020), at ultra-violet (UV) wavelengths with ULTRASAT (Sagiv et al. 2014), and in gamma-rays with CTA (Cherenkov Telescope Array Consortium et al. 2019; Carosi et al. 2021). These new instruments, in concert with the continuation of existing follow-up programs, will enable us to study the dynamic neutrino sky across the entire electromagnetic spectrum.

## ACKNOWLEDGEMENTS

R.S. and A.F. acknowledges support by the Initiative and Networking Fund of the Helmholtz Association through the Young Investigator Group program (A.F.). J.N. and S.R. acknowledges support by the Helmholtz Weizmann Research School on Multimessenger Astronomy, funded through the Initiative and Networking Fund of the

Helmholtz Association, DESY, the Weizmann Institute, the Humboldt University of Berlin, and the University of Potsdam.

Based on observations obtained with the Samuel Oschin Telescope 48-inch and the 60-inch Telescope at the Palomar Observatory as part of the Zwicky Transient Facility project. ZTF is supported by the National Science Foundation under Grant No. AST-1440341 and AST-2034437, and a collaboration including Caltech, IPAC, the Weizmann Institute for Science, the Oskar Klein Center at Stockholm University, the University of Maryland, the University of Washington, Deutsches Elektronen-Synchrotron and Humboldt University, Los Alamos National Laboratories, the TANGO Consortium of Taiwan, the University of Wisconsin at Milwaukee, Lawrence Berkeley National Laboratories, Trinity College Dublin, Lawrence Livermore National Laboratories, IN2P3, France, the University of Warwick, the University of Bochum, and Northwestern University. Operations are conducted by COO, IPAC, and UW. SED Machine is based upon work supported by the National Science Foundation under Grant No. 1106171. The ZTF forced-photometry service was funded under the Heising-Simons Foundation grant #12540303 (PI: Graham).

The data presented herein were obtained in part at the W. M. Keck Observatory, which is operated as a scientific partnership among the California Institute of Technology, the University of California and the National Aeronautics and Space Administration. The Observatory was made possible by the generous financial support of the W. M. Keck Foundation.

The authors wish to recognize and acknowledge the very significant cultural role and reverence that the summit of Maunakea has always had within the indigenous Hawaiian community. We are most fortunate to have the opportunity to conduct observations from this mountain.

Based on observations made with the Nordic Optical Telescope, owned in collaboration by the University of Turku and Aarhus University, and operated jointly by Aarhus University, the University of Turku and the University of Oslo, representing Denmark, Finland and Norway, the University of Iceland and Stockholm University at the Observatorio del Roque de los Muchachos, La Palma, Spain, of the Instituto de Astrofísica de Canarias. The data presented here were obtained in part with ALFOSC, which is provided by the Instituto de Astrofísica de Andalucía (IAA) under a joint agreement with the University of Copenhagen and NOT.

This research made use of Astropy, a community-developed core Python package for Astronomy (Astropy Collaboration et al. 2018, 2013). This research made use of Astroquery (Ginsburg et al. 2019), of the NASA/IPAC Extragalactic Database (NED) which is operated by the Jet Propulsion Laboratory, California Institute of Technology, under contract with the National Aeronautics and Space Administration.

## DATA AVAILABILITY

The data presented here, and the Python analysis code used to generate the figures and key results, can be found on Github at <https://github.com/robertdstein/nuztfpaper> and on Zenodo with DOI (coming soon...).

## REFERENCES

- Aartsen M. G., et al., 2015, *ApJ*, **811**, 52  
Aartsen M. G., et al., 2017, *Astroparticle Physics*, **92**, 30  
Aartsen M. G., et al., 2020, *Phys. Rev. Lett.*, **124**, 051103  
Abbasi R., et al., 2021, arXiv e-prints, p. arXiv:2111.10169

- Abolfathi B., et al., 2018, *ApJS*, **235**, 42
- Astropy Collaboration et al., 2013, *A&A*, **558**, A33
- Astropy Collaboration et al., 2018, *AJ*, **156**, 123
- Barbon R., Benetti S., Cappellaro E., Patat F., Turatto M., Iijima T., 1995, *A&AS*, **110**, 513
- Bednarek W., Protheroe R. J., 1999, *MNRAS*, **302**, 373
- Bellm E. C., et al., 2019, *PASP*, **131**, 018002
- Blaufuss E., 2018a, GCN Circular, 23214
- Blaufuss E., 2018b, GCN Circular, 23375
- Blaufuss E., 2018c, GCN Circular, 23398
- Blaufuss E., 2019a, GCN Circular, 23785
- Blaufuss E., 2019b, GCN Circular, 23876
- Blaufuss E., 2019c, GCN Circular, 24378
- Blaufuss E., 2019d, GCN Circular, 24674
- Blaufuss E., 2019e, GCN Circular, 24854
- Blaufuss E., 2019f, GCN Circular, 24910
- Blaufuss E., 2019g, GCN Circular, 25057
- Blaufuss E., 2019h, GCN Circular, 25806
- Blaufuss E., 2019i, GCN Circular, 26258
- Blaufuss E., 2019j, GCN Circular, 26276
- Blaufuss E., 2020a, GCN Circular, 27612
- Blaufuss E., 2020b, GCN Circular, 27787
- Blaufuss E., 2020c, GCN Circular, 27941
- Blaufuss E., 2020d, GCN Circular, 28163
- Blaufuss E., 2020e, GCN Circular, 28433
- Blaufuss E., 2020f, GCN Circular, 28509
- Blaufuss E., 2020g, GCN Circular, 28616
- Blaufuss E., 2020h, GCN Circular, 28887
- Blaufuss E., 2020i, GCN Circular, 28892
- Blaufuss E., 2020j, GCN Circular, 29102
- Blaufuss E., 2020k, GCN Circular, 29120
- Blaufuss E., 2021, GCN Circular, 29506
- Blaufuss E., Kintscher T., Lu L., Tung C. F., 2019, in 36th International Cosmic Ray Conference (ICRC2019). p. 1021 ([arXiv:1908.04884](https://arxiv.org/abs/1908.04884))
- Blondin S., Tonry J. L., 2007, *ApJ*, **666**, 1024
- Carosi A., et al., 2021, arXiv e-prints, p. [arXiv:2108.04309](https://arxiv.org/abs/2108.04309)
- Cherenkov Telescope Array Consortium et al., 2019, Science with the Cherenkov Telescope Array, doi:10.1142/10986.
- Evans P. A., et al., 2015, *MNRAS*, **448**, 2210
- Farrar G. R., Gruzinov A., 2009, *ApJ*, **693**, 329
- Ferrigno C., et al., 2021, *New Astron. Rev.*, **92**, 101595
- Flesch E. W., 2021, arXiv e-prints, p. [arXiv:2105.12985](https://arxiv.org/abs/2105.12985)
- Franckowiak A., et al., 2020, *ApJ*, **893**, 162
- Fremling C., et al., 2020, *ApJ*, **895**, 32
- Gaia Collaboration et al., 2018, *A&A*, **616**, A1
- Galama T. J., et al., 1998, *Nature*, **395**, 670
- Garrappa S., Buson S., Sinapius J., Kadl M., 2021a, The Astronomer's Telegram, **15099**, 1
- Garrappa S., Buson S., Franckowiak A., Giroletti M., Liodakis I., Nanci C., 2021b, *PoS, ICRC2021*, 956
- Ginsburg A., et al., 2019, *AJ*, **157**, 98
- Giommi P., Glauch T., Padovani P., Resconi E., Turcati A., Chang Y. L., 2020a, *MNRAS*, **497**, 865
- Giommi P., Padovani P., Oikonomou F., Glauch T., Paiano S., Resconi E., 2020b, *A&A*, **640**, L4
- Giommi P., Glauch T., Resconi E., 2020c, The Astronomer's Telegram, **13394**, 1
- Graham M. J., et al., 2019, *PASP*, **131**, 078001
- Guillochon J., Nicholl M., Villar V. A., Mockler B., Narayan G., Mandel K. S., Berger E., Williams P. K. G., 2018, *ApJS*, **236**, 6
- Hayasaki K., 2021, *Nature Astronomy*, **5**, 436
- Holmbo S., et al., 2019, The Astronomer's Telegram, **12661**
- IceCube Collaboration 2013, *Science*, **342**, 1242856
- IceCube Collaboration et al., 2018, *Science*, **361**, eaat1378
- Ivezic Z., et al., 2019, *ApJ*, **873**, 111
- Kadler M., et al., 2021a, arXiv e-prints, p. [arXiv:2108.00383](https://arxiv.org/abs/2108.00383)
- Kadler M., et al., 2021b, The Astronomer's Telegram, **15105**, 1
- Kasliwal M. M., et al., 2020, *ApJ*, **905**, 145
- Kiehlmann S., Hovatta T., Kadler M., Max-Moerbeck W., Readhead A. C. S., 2019, The Astronomer's Telegram, **12996**
- Kopper C., 2018, GCN Circular, 22669
- Kopper C., 2019a, GCN Circular, 23605
- Kopper C., 2019b, GCN Circular, 24028
- Kopper C., 2019c, GCN Circular, 24392
- Kowalski M., Mohr A., 2007, *Astroparticle Physics*, **27**, 533
- Krauss F., Gregoire T., Fox D. B., Kennea J., Evans P., 2020, The Astronomer's Telegram, **13395**, 1
- Lagunas Gualda C., 2020a, GCN Circular, 26802
- Lagunas Gualda C., 2020b, GCN Circular, 26832
- Lagunas Gualda C., 2020c, GCN Circular, 27719
- Lagunas Gualda C., 2020d, GCN Circular, 27950
- Lagunas Gualda C., 2020e, GCN Circular, 28411
- Lagunas Gualda C., 2020f, GCN Circular, 28468
- Lagunas Gualda C., 2020g, GCN Circular, 28504
- Lagunas Gualda C., 2020h, GCN Circular, 28532
- Lagunas Gualda C., 2020i, GCN Circular, 28715
- Lagunas Gualda C., 2020j, GCN Circular, 28889
- Lagunas Gualda C., 2020k, GCN Circular, 28927
- Lagunas Gualda C., 2020l, GCN Circular, 28969
- Lagunas Gualda C., 2020m, GCN Circular, 29012
- Lagunas Gualda C., 2021a, GCN Circular, 29454
- Lagunas Gualda C., 2021b, GCN Circular, 30153
- Lagunas Gualda C., 2021c, GCN Circular, 30468, 1
- Lagunas Gualda C., 2021d, GRB Coordinates Network, **31085**, 1
- Lagunas Gualda C., 2021e, GRB Coordinates Network, **31126**, 1
- Lagunas Gualda C., Ashida Y., Sharma A., Thomas H., 2021, *PoS, ICRC2021*, 1045
- Lien A., Sakamoto T., Gehrels N., Palmer D. M., Barthelmy S. D., Graziani C., Cannizzo J. K., 2014, *ApJ*, **783**, 24
- Lincetto M., 2021a, GRB Coordinates Network, **30862**, 1
- Lincetto M., 2021b, GRB Coordinates Network, **30957**, 1
- Lipunov V. M., et al., 2020, *ApJ*, **896**, L19
- Lourie N. P., et al., 2020, in Society of Photo-Optical Instrumentation Engineers (SPIE) Conference Series. p. 114479K ([arXiv:2102.01109](https://arxiv.org/abs/2102.01109)), doi:10.1117/12.2561210
- Lucarelli F., et al., 2019, *ApJ*, **870**, 136
- Lyman J. D., Bersier D., James P. A., Mazzali P. A., Eldridge J. J., Fraser M., Pian E., 2016, *MNRAS*, **457**, 328
- Mannheim K., 1993, *A&A*, **269**, 67
- Masci F. J., et al., 2019, *PASP*, **131**, 018003
- Morgan R., et al., 2019, *ApJ*, **883**, 125
- Murase K., Thompson T. A., Lacki B. C., Beacom J. F., 2011, *Phys. Rev. D*, **84**, 043003
- Nakar E., 2015, *ApJ*, **807**, 172
- Necker J., Stein R., Weimann S., Reusch S., Franckowiak A., 2021, GCN Circular, **30349**
- Necker J., de Jaeger T., Stein R., Franckowiak A., Shappee B., Kowalski M., et al., 2022, arXiv e-prints
- Nordin J., et al., 2019, *A&A*, **631**, A147
- Oke J. B., et al., 1995, *PASP*, **107**, 375
- Padovani P., Resconi E., Giommi P., Arsioli B., Chang Y. L., 2016, *MNRAS*, **457**, 3582
- Paliya V. S., Böttcher M., Olmo-García A., Domínguez A., Gil de Paz A., Franckowiak A., Garrappa S., Stein R., 2020, *ApJ*, **902**, 29
- Pan-Starrs Collaboration et al., 2019, *A&A*, **626**, A117
- Pastorello A., et al., 2006, *MNRAS*, **370**, 1752
- Perley D. A., et al., 2020, *ApJ*, **904**, 35
- Petropoulou M., Oikonomou F., Mastichiadis A., Murase K., Padovani P., Vasilopoulos G., Giommi P., 2020, *ApJ*, **899**, 113
- Plavin A., Kovalev Y. Y., Kovalev Y. A., Troitsky S., 2020, *ApJ*, **894**, 101
- Plavin A. V., Kovalev Y. Y., Kovalev Y. A., Troitsky S. V., 2021, *ApJ*, **908**, 157
- Reguitti A., et al., 2019, The Astronomer's Telegram, **13133**
- Reusch S., 2020, simeonreusch/ztfpps: Release (3), doi:10.5281/zenodo.4049711, <https://doi.org/10.5281/zenodo.4049711>

859 Reusch S., Stein R., 2020a, GCN Circular, 26747  
860 Reusch S., Stein R., 2020b, GCN Circular, 26813  
861 Reusch S., Stein R., 2020c, GCN Circular, 26816  
862 Reusch S., Stein R., Franckowiak A., 2020a, GCN Circular, 27721  
863 Reusch S., Stein R., Franckowiak A., Gezari S., 2020b, GCN Circular, 27872  
864 Reusch S., Stein R., Franckowiak A., Sollerman J., Schweyer T., Barbarino  
865 C., 2020c, GCN Circular, 27910  
866 Reusch S., Stein R., Franckowiak A., Necker J., Sollerman J., Barbarino C.,  
867 Schweyer T., 2020d, GCN Circular, 27980  
868 Reusch S., Stein R., Franckowiak A., 2020e, GCN Circular, 28005  
869 Reusch S., Stein R., Franckowiak A., Andreoni I., Coughlin M., 2020f, GCN  
870 Circular, 28441  
871 Reusch S., Stein R., Franckowiak A., Schulze S., Sollerman J., 2020g, GCN  
872 Circular, 28465  
873 Reusch S., Stein R., Weimann S., Franckowiak A., 2020h, GCN Circular,  
874 28520  
875 Reusch S., Weimann S., Stein R., Franckowiak A., 2020i, GCN Circular,  
876 28609  
877 Reusch S., Weimann S., Stein R., Franckowiak A., 2020j, GCN Circular,  
878 29031  
879 Reusch S., et al., 2021a, arXiv e-prints, p. [arXiv:2111.09390](https://arxiv.org/abs/2111.09390)  
880 Reusch S., Weimann S., Stein R., Coughlin M., Franckowiak A., 2021b, GCN  
881 Circular, 29461  
882 Rodrigues X., Garrappa S., Gao S., Paliya V. S., Franckowiak A., Winter W.,  
883 2021, *ApJ*, 912, 54  
884 Sagiv I., et al., 2014, *AJ*, 147, 79  
885 Santander M., 2019a, GCN Circular, 24981  
886 Santander M., 2019b, GCN Circular, 25402  
887 Santander M., 2019c, GCN Circular, 26620  
888 Santander M., 2020a, GCN Circular, 27651  
889 Santander M., 2020b, GCN Circular, 27997  
890 Santander M., 2020c, GCN Circular, 28575  
891 Santander M., 2021a, GCN Circular, 29688  
892 Santander M., 2021b, GCN Circular, 29951  
893 Santander M., 2021c, GCN Circular, 29976  
894 Santander M., 2021d, GCN Circular, 30026  
895 Santander M., 2021e, GCN Circular, 30056  
896 Santander M., 2021f, GCN Circular, 30342  
897 Santander M., 2021g, GCN Circular, 30559, 1  
898 Santander M., 2021h, GCN Circular, 30627, 1  
899 Santander M., 2021i, GRB Coordinates Network, 31093, 1  
900 Santander M., 2021j, GRB Coordinates Network, 31110, 1  
901 Santander M., 2021k, GRB Coordinates Network, 31195, 1  
902 Santander M., Buson S., 2021, The Astronomer's Telegram, 15102, 1  
903 Satalecka K., Bernardini E., Dorner D., Kukec Mezek G., Jin W., 2021, arXiv  
904 e-prints, p. [arXiv:2109.04350](https://arxiv.org/abs/2109.04350)  
905 Savchenko S. S., Larionova E. G., Grisnina T. S., 2021, The Astronomer's  
906 Telegram, 15021, 1  
907 Senno N., Murase K., Mészáros P., 2016, *Phys. Rev. D*, 93, 083003  
908 Stein R., 2019a, GCN Circular, 25225  
909 Stein R., 2019b, GCN Circular, 25802  
910 Stein R., 2019c, GCN Circular, 25913  
911 Stein R., 2019d, GCN Circular, 26341  
912 Stein R., 2019e, GCN Circular, 26435  
913 Stein R., 2020a, GCN Circular, 26655  
914 Stein R., 2020b, GCN Circular, 26696  
915 Stein R., 2020c, GCN Circular, 27235  
916 Stein R., 2020d, GCN Circular, 27534  
917 Stein R., 2020e, GCN Circular, 27865  
918 Stein R., 2020f, GCN Circular, 28210  
919 Stein R., Reusch S., 2020, GCN Circular, 26667  
920 Stein R., et al., 2019a, The Astronomer's Telegram, 12730  
921 Stein R., et al., 2019b, The Astronomer's Telegram, 12879  
922 Stein R., Franckowiak A., Kasliwal M. M., Andreoni I., Coughlin M., Singer  
923 L. P., Masci F., van Velzen S., 2019c, The Astronomer's Telegram, 12974  
924 Stein R., Franckowiak A., Kowalski M., Kasliwal M., 2019d, GCN Circular,  
925 25824

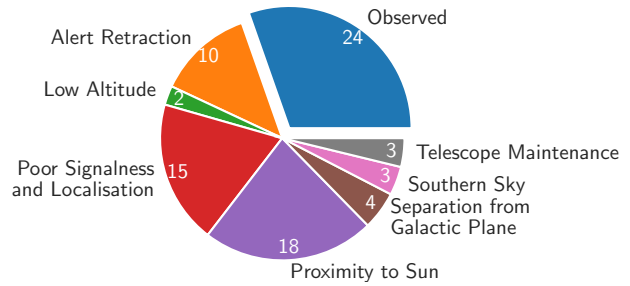


**Figure A1.** Breakdown of the neutrino follow-up program, as of 2021 Dec 31.

926 Stein R., Franckowiak A., Necker J., Gezari S., van Velzen S., 2019e, GCN  
927 Circular, 25929  
928 Stein R., Necker J., Bradascio F., simonegarrappa 2020a, icecube/flarestack,  
929 [doi:10.5281/zenodo.3619383](https://doi.org/10.5281/zenodo.3619383), <https://doi.org/10.5281/zenodo.3619383>  
930  
931 Stein R., Reusch S., Weimann S., Coughlin M., 2020b, GCN Circular, 28757  
932 Stein R., Weimann S., Reusch S., Franckowiak A., 2020c, GCN Circular,  
933 29172  
934 Stein R., et al., 2021a, *Nature Astronomy*,  
935 Stein R., Reusch S., Necker J., 2021b, desy-multimessenger/nuztf: v2.1.0  
936 Release, [doi:10.5281/zenodo.5217976](https://doi.org/10.5281/zenodo.5217976), <https://doi.org/10.5281/zenodo.5217976>  
937  
938 Stein R., Weimann S., Necker J., Reusch S., Franckowiak A., Zwicky Transient  
939 Facility Growth Collaboration 2021c, GCN Circular, 29999  
940 Stein R., Weimann S., Reusch S., Necker J., Franckowiak A., Coughlin M.,  
941 Zwicky Transient Facility collaboration Global Relay of Observatories  
942 Watching Transients Happen Collaboration 2021d, GCN Circular, 30644,  
943 1  
944 Stern D., et al., 2012, *ApJ*, 753, 30  
945 Stoughton C., et al., 2002, *AJ*, 123, 485  
946 Strolger L.-G., et al., 2015, *ApJ*, 813, 93  
947 Strotjohann N. L., Kowalski M., Franckowiak A., 2019, *A&A*, 622, L9  
948 Taboada I., 2018, GCN Circular, 23338  
949 Taboada I., 2019, GCN Circular, 23918  
950 Taubenberger S., et al., 2006, *MNRAS*, 371, 1459  
951 Waxman E., Bahcall J., 1997, *Phys. Rev. Lett.*, 78, 2292  
952 Weimann S., Stein R., Reusch S., Franckowiak A., 2020a, GCN Circular,  
953 28551  
954 Weimann S., Stein R., Reusch S., Franckowiak A., 2020b, GCN Circular,  
955 28989  
956 Weimann S., Reusch S., Necker J., Stein R., Franckowiak A., Zwicky Transient  
957 Facility Growth Collaboration 2021, GRB Coordinates Network,  
958 30870, 1  
959 Wright E. L., et al., 2010, *AJ*, 140, 1868  
960 Zhirkov K., et al., 2021, The Astronomer's Telegram, 15098, 1  
961 van Velzen S., et al., 2021, arXiv e-prints, p. [arXiv:2111.09391](https://arxiv.org/abs/2111.09391)

## APPENDIX A: NOT FOLLOWED UP

962  
963 Those alerts not observed by ZTF are summarised in Table A1. Of  
964 those 55 alerts not followed up, the primary reasons were proximity  
965 to the Sun (18/55), alerts with poor localisation and low astrophysical  
966 probability (15/55) and alert retraction (10/55). The full breakdown  
967 of neutrino observations statistics can be seen in Figure A1.

968 This paper has been typeset from a  $\text{\TeX}/\text{\LaTeX}$  file prepared by the author.

Cause	Events	
Alert Retraction	IC180423A (Kopper 2018)	
	IC181031A (Blaufuss 2018c)	
	IC190205A (Blaufuss 2019b)	
	IC190529A (Blaufuss 2019d)	
	IC200120A (Lagunas Gualda 2020b)	
	IC200728A (Blaufuss 2020d)	
	IC201115B (Blaufuss 2020i)	
	IC210213A (Blaufuss 2021)	
	IC210322A (Santander 2021a)	
	IC210519A (Santander 2021e)	
	Proximity to Sun	IC180908A (Blaufuss 2018a)
		IC181014A (Taboada 2018)
		IC190124A (Blaufuss 2019a)
IC190704A (Santander 2019a)		
IC190712A (Blaufuss 2019g)		
IC190819A (Santander 2019b)		
IC191119A (Blaufuss 2019i)		
IC200227A (Stein 2020c)		
IC200421A (Blaufuss 2020a)		
IC200615A (Lagunas Gualda 2020d)		
IC200806A (Stein 2020f)		
IC200921A (Lagunas Gualda 2020f)		
IC200926B (Blaufuss 2020f)		
IC201014A (Blaufuss 2020g)		
IC201115A (Lagunas Gualda 2020j)		
IC201221A (Blaufuss 2020j)		
IC211117A (Santander 2021i)		
IC211123A (Santander 2021j)		
Low Altitude	IC191215A (Stein 2019e)	
	IC211023A (Lincetto 2021b)	
Southern Sky	IC190104A (Kopper 2019a)	
	IC190331A (Kopper 2019b)	
	IC190504A (Kopper 2019c)	
Separation from Galactic Plane	IC201114A (Blaufuss 2020h)	
	IC201120A (Lagunas Gualda 2020k)	
	IC210516A (Santander 2021d)	
	IC210730A (Santander 2021g)	
Poor Signalness and Localisation	IC190221A (Taboada 2019)	
	IC190629A (Blaufuss 2019f)	
	IC190922A (Stein 2019b)	
	IC191122A (Blaufuss 2019j)	
	IC191204A (Stein 2019d)	
	IC191231A (Santander 2019c)	
	IC200410A (Stein 2020d)	
	IC200425A (Santander 2020a)	
	IC200523A (Blaufuss 2020b)	
	IC200614A (Blaufuss 2020c)	
	IC200911A (Lagunas Gualda 2020e)	
	IC210503A (Santander 2021b)	
	IC210608A (Lagunas Gualda 2021b)	
	IC210717A (Lagunas Gualda 2021c)	
IC211125A (Lagunas Gualda 2021e)		
Telescope Maintenance	IC181023A (Blaufuss 2018b)	
	IC211116A (Lagunas Gualda 2021d)	
	IC211208A (Santander 2021k)	

**Table A1.** Summary of the 55 neutrino alerts that were not followed up by ZTF since survey start on 2018 March 20.

ZTF Name	IAU Name	Classification	Peak Magnitude
ZTF19aatqcwq	–	AGN Variability	20.6 (g)
ZTF19aatqlwq	–	AGN Variability	21.2 (r)

**Table A2.** Candidates for IC190503A.

ZTF Name	IAU Name	Classification	Peak Magnitude
ZTF18abolwbb	–	AGN Variability	19.4 (r)
ZTF18abueqkl	AT2020kqj	AGN Variability	19.3 (g)
ZTF18acehkni	–	AGN Variability	19.4 (r)
ZTF18actxhc	–	AGN Variability	18.0 (g)
ZTF19aadaszg	SN2019rg	SN Ia	15.9 (r)
ZTF19aawnawu	–	AGN Variability	20.0 (g)
ZTF19aaycone	–	AGN Variability	17.9 (g)
ZTF19aaycool	–	AGN Variability	20.3 (g)
ZTF19aaycosc	–	AGN Variability	19.3 (r)
ZTF19aaycoxd	–	AGN Variability	20.3 (g)
ZTF19abahiwr	AT2019izf	Unclassified	19.5 (r)
ZTF19abahiya	–	Unclassified	19.6 (r)
ZTF19abahizn	–	AGN Variability	19.7 (g)
ZTF19abahjcp	–	AGN Variability	20.2 (g)
ZTF19abahlep	–	Unclassified	20.8 (r)
ZTF19abahlka	–	AGN Variability	19.8 (i)
ZTF19abajnby	–	AGN Variability	20.0 (r)

**Table A3.** Candidates for IC190619A.

ZTF Name	IAU Name	Classification	Peak Magnitude
ZTF19aanlzzk	–	Artefact	13.8 (g)

**Table A4.** Candidates for IC190730A.

ZTF Name	IAU Name	Classification	Peak Magnitude
ZTF18acekfly	AT2019kkd	AGN Variability	18.5 (r)
ZTF19abcejyp	AT2019kkp	AGN Variability	19.3 (r)
ZTF19abxtupj	AT 2019pqh	SN II/Ib	20.3 (r)

**Table A5.** Candidates for IC190922B.

ZTF Name	IAU Name	Classification	Peak Magnitude
ZTF18ablvxkp	–	AGN Variability	19.3 (r)
ZTF18absoqfm	–	AGN Variability	19.0 (g)
ZTF19aapreis	AT2019dsg	TDE	17.8 (g)
ZTF19abassjx	–	AGN Variability	19.4 (i)
ZTF19abcdynm	–	AGN Variability	20.5 (g)
ZTF19abexshr	–	AGN Variability	20.2 (r)
ZTF19abjflkj	–	AGN Variability	20.9 (g)
ZTF19abjflnc	–	AGN Variability	19.2 (i)
ZTF19abjflrg	–	AGN Variability	21.3 (g)
ZTF19abjfmem	–	AGN Variability	21.5 (g)
ZTF19abwaurq	–	Unclassified	19.5 (r)
ZTF19abzkexb	SN2019qhl	SN Ia	18.9 (g)
ZTF19acbpqfn	AT2019rsj	Unclassified	20.4 (g)
ZTF19acbpqui	–	Unclassified	20.5 (g)
ZTF19acbwpgs	–	AGN Variability	19.9 (g)
ZTF19acbxahc	–	Unclassified	21.1 (g)
ZTF19acbxanz	–	Unclassified	20.6 (r)
ZTF19acbxajq	–	Unclassified	20.5 (r)
ZTF19acbxauk	–	Unclassified	20.8 (g)
ZTF19acbxbjq	AT2019rsk	Unclassified	20.3 (g)
ZTF19accnqlc	–	Unclassified	20.2 (r)

**Table A6.** Candidates for IC191001A.

ZTF Name	IAU Name	Classification	Peak Magnitude
ZTF18aaidhnq	–	AGN Variability	18.1 (r)
ZTF18acekyg	–	AGN Variability	19.0 (g)
ZTF18adgvgdk	–	AGN Variability	19.3 (g)
ZTF19aangwsm	–	Artefact	19.8 (g)
ZTF19aapsgb	–	AGN Variability	18.8 (r)
ZTF19aarohku	–	AGN Variability	19.8 (r)
ZTF19acmwlds	AT 2019yfm	Unclassified	19.7 (g)
ZTF19adcdxgc	–	AGN Variability	19.6 (g)
ZTF20aaeunmm	–	AGN Variability	20.4 (g)
ZTF20aaeuufe	AT 2019yii	Unclassified	20.4 (r)
ZTF20aaevfrv	–	Star	20.7 (g)
ZTF20aaevfth	AT 2020ux	Unclassified	21.2 (g)
ZTF20aaevfwa	AT 2019zxa	Unclassified	20.6 (r)
ZTF20aaevgt	AT 2020uw	Artefact	20.5 (r)
ZTF20aagvve	–	Artefact	19.7 (r)
ZTF20aagvvh	–	Artefact	19.8 (r)
ZTF20aagvvhk	–	Artefact	19.9 (r)
ZTF20aagvvn	–	Artefact	20.0 (r)
ZTF20aagwcup	AT2020dte	Artefact	19.9 (r)
ZTF20aagwcuq	–	Unclassified	20.0 (r)
ZTF20aagwcuu	–	Unclassified	20.0 (r)
ZTF20aagwcuw	–	Unclassified	19.9 (r)
ZTF20aagxfta	–	Unclassified	19.9 (g)

**Table A7.** Candidates for IC200109A.

ZTF Name	IAU Name	Classification	Peak Magnitude
ZTF19acxopgh	AT 2019zyu	Unclassified	19.4 (r)
ZTF19adceqeb	–	AGN Variability	19.6 (g)
ZTF20aacztcp	AT2020ko	AGN Variability	19.0 (r)
ZTF20aaglixd	AT 2020agt	Unclassified	21.2 (g)

**Table A8.** Candidates for IC200117A.

ZTF Name	IAU Name	Classification	Peak Magnitude
ZTF18aazvbyj	–	Star	17.5 (r)
ZTF18abjnqos	–	Star	12.9 (r)
ZTF18abmfxbh	–	Artefact	17.5 (r)
ZTF18abmfzmm	–	Artefact	17.1 (r)
ZTF19acgpzgi	–	Artefact	15.5 (g)
ZTF20aazqsfe	–	Star	19.6 (g)

**Table A9.** Candidates for IC200512A.

ZTF Name	IAU Name	Classification	Peak Magnitude
ZTF18aaimsgg	AT2018lnq	Artefact	16.6 (r)
ZTF18aamjques	AT2020llg	AGN Variability	16.9 (r)
ZTF18aaneyxs	–	Artefact	14.6 (r)
ZTF18aavecmo	AT2020llh	AGN Flare	19.6 (i)
ZTF18aazkjyd	–	Artefact	14.7 (r)
ZTF18abrwwqr	AT2020lli	AGN Flare	19.6 (g)
ZTF19aakonfhr	AT2020llj	AGN Variability	20.4 (r)
ZTF19aascfca	–	AGN Variability	20.7 (g)
ZTF19aascffj	–	AGN Variability	20.0 (g)
ZTF19aatubsj	SN 2019fdr	TDE	17.9 (i)
ZTF19abregmj	AT2020llk	AGN Variability	19.9 (g)
ZTF20aaiifyfd	AT2020lll	AGN Variability	19.9 (g)
ZTF20aaiifyrs	SN2020awa	SN Ia	17.0 (r)
ZTF20aarbkttd	SN2020djn	SN II	18.0 (i)
ZTF20aavnpuq	AT2020idu	Dwarf Nova	15.9 (i)
ZTF20aawyens	AT2020lpp	AGN Variability	19.7 (i)
ZTF20aaxcdok	AT2020lpq	Unclassified	20.1 (r)
ZTF20aaxyglz	AT2020llm	AGN Variability	20.3 (g)
ZTF20abaofgx	AT2020lpr	AGN Variability	19.9 (r)
ZTF20abbpkpa	AT 2020lam	SN II	18.8 (g)
ZTF20abcnrcb	–	AGN Variability	19.3 (g)
ZTF20abdnovz	–	Star	21.3 (r)
ZTF20abdnowa	AT2020lln	Artefact	20.7 (g)
ZTF20abdnowp	AT2020llo	Unclassified	21.1 (g)
ZTF20abdnowx	–	AGN Variability	21.3 (g)
ZTF20abdnoxz	–	AGN Variability	20.3 (g)
ZTF20abdnoxm	AT2020llp	Unclassified	20.8 (g)
ZTF20abdnoyu	AT2020lps	Unclassified	21.4 (g)
ZTF20abdnozq	AT2020llq	AGN Variability	20.6 (r)
ZTF20abdnuae	AT2020lpt	Unclassified	20.9 (g)
ZTF20abdnubp	AT2020llr	AGN Variability	20.7 (r)
ZTF20abdnubq	AT 2020lpw	AGN Variability	21.0 (r)
ZTF20abdnubv	AT 2020lpx	Unclassified	21.0 (g)
ZTF20abdnubo	AT 2020lls	SN Ic	19.0 (r)
ZTF20abdqzjl	–	Star	20.4 (r)
ZTF20abdqzjr	–	AGN Variability	21.1 (r)
ZTF20abdqzqk	AT 2020lpu	Star	20.7 (g)
ZTF20abdqzkr	–	AGN Variability	21.1 (g)
ZTF20abdrnjw	–	Star	21.3 (r)
ZTF20abdrnlq	AT2020lpv	Unclassified	20.9 (r)
ZTF20abdrnmp	–	AGN Variability	21.6 (r)

**Table A10.** Candidates for IC200530A.

ZTF Name	IAU Name	Classification	Peak Magnitude
ZTF18acvhwtf	AT 2020ncs	AGN Variability	19.7 (r)
ZTF20abgvabi	AT 2020ncr	AGN Variability	20.2 (r)

**Table A11.** Candidates for IC200620A.



ZTF Name	IAU Name	Classification	Peak Magnitude
ZTF18accxxf	AT2020tnn	AGN Variability	19.7 (g)
ZTF18adbbnry	AT2020tnn	AGN Variability	19.8 (g)
ZTF20acaapwk	SN2020tno	SN Ia	18.9 (r)
ZTF20acaapwn	–	Unclassified	21.0 (g)
ZTF20acaapwo	AT2020tnp	Unclassified	20.4 (r)
ZTF20acayuno	–	AGN Variability	21.1 (r)

**Table A12.** Candidates for IC200916A.

ZTF Name	IAU Name	Classification	Peak Magnitude
ZTF18achvmdz	–	AGN Variability	18.9 (i)
ZTF18acwfrle	–	Star	15.4 (g)

**Table A13.** Candidates for IC200926A.

ZTF Name	IAU Name	Classification	Peak Magnitude
ZTF20aamoxyt	–	AGN Flare	19.8 (g)

**Table A14.** Candidates for IC200929A.

ZTF Name	IAU Name	Classification	Peak Magnitude
ZTF18abmkdiy	AT2019cvb	AGN Variability	18.7 (i)
ZTF20abfaado	AT2020nbr	Star	19.3 (i)
ZTF20acinqzo	–	AGN Variability	19.6 (i)
ZTF20acmxnpa	AT2020ybb	Unclassified	20.6 (g)

**Table A15.** Candidates for IC201021A.

ZTF Name	IAU Name	Classification	Peak Magnitude
ZTF17aadmvpm	–	Artefact	16.1 (g)
ZTF18abxrpgu	AT2021ury	AGN Flare	18.8 (r)
ZTF18achpvr1	–	AGN Variability	19.1 (r)
ZTF19aaagxcv	–	AGN Variability	18.4 (g)
ZTF20aceidvg	–	AGN Variability	19.7 (g)
ZTF20acmnnwf	–	AGN Variability	19.9 (r)
ZTF20acuqdeu	AT2020aehs	Unclassified	19.8 (g)
ZTF20acxbkpz	–	Unclassified	20.5 (r)

**Table A16.** Candidates for IC201130A.

ZTF Name	IAU Name	Classification	Peak Magnitude
ZTF18abwhosy	–	AGN Variability	19.3 (r)
ZTF20abvxjup	–	AGN Variability	20.0 (g)
ZTF20acycunv	SN2020addp	SN IIP	19.4 (r)

**Table A17.** Candidates for IC201209A.

ZTF Name	IAU Name	Classification	Peak Magnitude
ZTF19aaapmca	–	AGN Variability	18.6 (r)
ZTF19aailrrn	–	AGN Variability	20.0 (g)
ZTF19aasfvho	–	AGN Variability	19.4 (g)
ZTF19aasfvqm	–	AGN Flare	18.2 (r)
ZTF20aadynqa	–	AGN Variability	20.1 (g)
ZTF20aaajcpde	–	AGN Variability	19.5 (g)
ZTF21aafmkun	–	AGN Variability	19.4 (r)
ZTF21aajxjmv	–	Star	21.3 (r)
ZTF21aajxjmy	–	Star	21.1 (g)
ZTF21aajxjnb	–	AGN Variability	22.1 (g)
ZTF21aajxjnc	–	AGN Variability	21.7 (g)
ZTF21aajxjrn	–	AGN Variability	20.1 (r)
ZTF21aajxjrv	AT2021clu	Unclassified	20.9 (r)
ZTF21aajxjry	AT2021clv	Unclassified	21.5 (r)
ZTF21aajxjsa	–	AGN Variability	21.7 (r)
ZTF21aajxkls	–	AGN Variability	21.1 (g)
ZTF21aakiqpp	–	Star	22.1 (g)

**Table A18.** Candidates for IC210210A.

ZTF Name	IAU Name	Classification	Peak Magnitude
ZTF19aadzayi	–	Star	15.0 (r)
ZTF19aawqcum	–	AGN Variability	19.1 (g)
ZTF20abhfiyd	–	Star	19.6 (g)
ZTF20acinxvv	–	Unclassified	21.0 (r)
ZTF20acinwlt	–	AGN Variability	21.0 (r)
ZTF21aaiuekm	–	Star	19.5 (g)

**Table A19.** Candidates for IC210510A.

ZTF Name	IAU Name	Classification	Peak Magnitude
ZTF18abteipt	AT2019gnu	AGN Variability	17.1 (r)
ZTF21abecljv	AT2021osi	AGN Variability	19.8 (i)
ZTF21abllruf	–	Artefact	17.5 (i)

**Table A20.** Candidates for IC210629A.

ZTF Name	IAU Name	Classification	Peak Magnitude
ZTF20abjezpo	–	Star	19.7 (r)
ZTF21absmcwm	–	AGN Variability	20.8 (g)

**Table A21.** Candidates for IC210811A.